New probe of magnetic fields in the prereionization epoch. I. Formalism

Tejaswi Venumadhav, Antonija Oklopčić, Vera Gluscevic, Abhilash Mishra, and Christopher M. Hirata

A new probe of magnetic fields in the pre-reionization epoch: I. Formalism

Tejaswi Venumadhav,[1,2] Antonija Oklopčić,[1] Vera Gluscevic,[2] Abhilash Mishra,[1] and Christopher M. Hirata[3]

[1] *Theoretical Astrophysics Including Relativity (TAPIR),*
Caltech M/C 350-17, Pasadena, California 91125, USA
[2] *School of Natural Sciences (SNS), Institute for Advanced Study,*
Einstein Drive, Princeton, New Jersey 08540, USA
[3] *Center for Cosmology and Astroparticle Physics (CCAPP),*
The Ohio State University, 191 West Woodruff Lane, Columbus, Ohio 43210, USA

We propose a method of measuring extremely weak magnetic fields in the intergalactic medium prior to and during the epoch of cosmic reionization. The method utilizes the Larmor precession of spin-polarized neutral hydrogen in the triplet state of the hyperfine transition. This precession leads to a systematic change in the brightness temperature fluctuations of the 21-cm line from the high-redshift universe, and thus the statistics of these fluctuations encode information about the magnetic field the atoms are immersed in. The method is most suited to probing fields that are coherent on large scales; in this paper, we consider a homogenous magnetic field over the scale of the 21-cm fluctuations. Due to the long lifetime of the triplet state of the 21-cm transition, this technique is naturally sensitive to extremely weak field strengths, of order 10^{-19} G at a reference redshift of ~ 20 (or 10^{-21} G if scaled to the present day). Therefore, this might open up the possibility of probing primordial magnetic fields just prior to reionization. If the magnetic fields are much stronger, it is still possible to use this method to infer their direction, and place a lower limit on their strength. In this paper (Paper I in a series on this effect), we perform detailed calculations of the microphysics behind this effect, and take into account all the processes that affect the hyperfine transition, including radiative decays, collisions, and optical pumping by Lyman-α photons. We conclude with an analytic formula for the brightness temperature of linear-regime fluctuations in the presence of a magnetic field, and discuss its limiting behavior for weak and strong fields.

I. INTRODUCTION

Magnetic fields (MFs) are seen in astrophysical structures on a wide range of observable scales, both in the local universe [1, 2] and at high redshifts [3]. Typical field strengths in galaxies and galaxy clusters are a few to a few tens of μG, with coherence lengths of up to hundreds of kpc [4]. However, properties of the intergalactic MFs on even larger length scales are largely unknown.

The leading paradigm for the origin of large-scale cosmic MFs assumes some kind of amplification and dynamo-based sustaining of weak seed fields [5]. These seed fields may originate from mechanisms effective during structure formation, or could be primordial remnants from the early universe (see, for example, Refs. [5–9]). The search for primordial magnetic fields (PMFs) is an active area of investigation in astrophysics and cosmology, as their observation would open up a new window into the physics of the early universe and possibly provide an entirely unexplored source of information about inflationary and pre-reheating processes.

Current upper limits on large-scale MFs come from several different observations, and are on the order of 10^{-9} G. They are derived from the limits on Faraday rotation of the cosmic-microwave-background (CMB) polarization [10] and of the radio emission from distant quasars [11], measurements of the CMB temperature anisotropies [12], limits on CMB spectral distortions [13], and various observations of large-scale structure (LSS) [14].

More recently, observations of TeV sources by the Fermi mission have been interpreted as implying the existence of magnetic fields stronger than 10^{-15} G with Mpc scale coherence lengths, in local LSS voids [15–17]. Plasma instabilities might avoid these bounds by eliminating the expected cascade of lower-energy gamma rays [18], but recent calculations indicate these instabilities might saturate, and thus challenge the viability of this argument [19, 20] (but see also Ref. [21]). The lower limit may also be reduced if the TeV emission timescale is short, since the arrival of the lower-energy cascade photons is delayed relative to the direct TeV photons [22, 23].

Most of these methods are sensitive to the integrated effect of MFs along a line of sight, and thus can be contaminated by low-redshift magnetic fields of astrophysical origin — for instance, those carried by galactic winds (for a notable exception, see Ref. [24] which probes local fields using statistical correlations in the gamma ray sky). Moreover, these methods optimally detect fields that are stronger than typical expectations for PMFs. Thus a definitive probe of PMFs needs to have the following features:

- The ability to isolate the effects of fields at different redshifts. In particular, sensitivity at high redshifts (prior to, or at the dawn of structure formation).

- Sensitivity to extremely low field strengths. Inflationary, post-inflationary, and structure-formation related mechanisms typically generate seed fields with strengths in the range 10^{-30}–10^{-15} G [7, 9].

- The ability to recover the MF power spectrum, whose features might give insight into the specifics of the process of magnetogenesis.

This is Paper I of a series that proposes a new observational probe of magnetic fields, which has all the desired properties listed above. In this Paper, we lay out the details of the microphysical calculation of the 21-cm signal in presence of the magnetic fields. In Paper II of this series [25], we present a minimum-variance formalism necessary to estimate the field strength with 21-cm tomography observations, and forecast sensitivity of future experiments to detecting two different MF configurations using this method.

The method discussed here is based on the effect of global MFs on the redshifted 21-cm emission from neutral hydrogen prior to and during the epoch of cosmic reionization (EoR), whose measurement is the goal of a number of low-frequency radio arrays, such as MWA [26], PAPER [27], HERA [28], LOFAR [29], LEDA [30], SKA [31], and others. The 21-cm signal allows insight into very high redshifts (in the approximate range $7 < z < 30$), including early epochs where the intergalactic medium (IGM) was just beginning to be affected by stellar feedback.

This method relies on the availability of internal (spin) degrees of freedom to hydrogen atoms in the triplet state of the ground hyperfine transition. As we show in the body of the paper, an anisotropic radiation field spin-polarizes these levels (also see previous work in Refs. [32–36]). Such anisotropies are naturally present in the early universe due to density fluctuations in the neutral gas. In the presence of a background magnetic field, the Larmor precession of the atoms leads to a characteristic signature in the 21-cm brightness temperature. In particular, a homogenous magnetic field breaks the statistical isotropy of the measured two-point correlation functions of the brightness temperature. This effect is inherently sensitive to extremely weak MFs, smaller than $\sim 10^{-19}$ G at a reference redshift $z \sim 20$.[1] This remarkable sensitivity is due to the long lifetime of the excited state, during which even very slow precession results in a substantial change in the direction of the emitted radiation.

The rest of this paper is organized as follows. We give some background about 21-cm cosmology and the Hanle effect (which is closely related to the effect considered in this paper) in Sections II A and II B. We then introduce the effect in a simple, semi-classical manner in Section III. We lay out the notation and formalism we use in Section IV, including our description of spin-polarized atoms in IV A and the anisotropic radiation field in the vicinity of the 21-cm transition in IV B. Next, we study the excitation and de-excitation of the atoms

by the 21-cm radiation in Section V. We compute the rates of de-polarization by competing non-radiative processes in Section VI, with VI B and VI C addressing spin-exchange collisions and optical pumping by Lyman-α photons, respectively. We describe the radiative transfer of 21-cm photons in Section VII. We put together all these results and calculate the resulting change in the brightness-temperature fluctuations in Section VIII. Finally, we summarize the paper and lay out our conclusions in Section IX. Various technical details involved in the computations are collected into the appendices.

II. BACKGROUND

A. 21-cm cosmology basics

The 21-cm line of neutral hydrogen corresponds to the transition between the hyperfine sublevels of its ground state, whose origin is the interaction between the spins of the proton and the electron. This interaction reorganizes the four possible spin states of the electron and proton into singlet and triplet levels, which are separated by an energy gap of 5.9×10^{-6} eV, corresponding to radiation with a wavelength of 21.1 cm (or a frequency of 1420 MHz), in the rest frame.

In the early stages of the EoR, the universe was still mostly neutral, and fluctuations in the brightness temperature of the 21-cm line were mainly driven by (mostly Gaussian) density fluctuations. This stage lends itself to a very precise statistical description, allowing us to get a good handle on the expected 21-cm signal from the corresponding redshifts [37].

The first generation of EoR experiments, such as the MWA, PAPER, and LOFAR, aim to achieve a statistical detection of the 21-cm signal from the EoR. Second generation experiments, such as the SKA and future phases of HERA, planned to come online within the next couple of decades, aim to perform detailed tomography of the IGM out to $z \sim 30$. Future 21-cm observations of the high-redshift universe can open up a new frontier in cosmology, with a sample volume far exceeding that probed with current observations. Several authors have suggested that cosmological 21-cm radiation could be used to detect primordial magnetic fields via their dynamical effects on density and gas temperature fluctuations [38–40]. The method proposed here is sensitive to much weaker fields than those investigated by other authors.

The conventional appeal of 21-cm observations is the availability of redshift information (in contrast to other probes of the very early universe, such as the CMB), the access to small-scale modes (Silk damped in the CMB and altered by nonlinear evolution today), and the consequent large number of accessible modes [41]. The effect studied in this paper relies on another aspect of the transition: in the triplet state, the net magnetic moment of the atom (which is dominated by the magnetic moment

---

[1] Note that a "frozen" magnetic field should scale as $\propto (1+z)^2$ due to flux conservation; the comoving field strength, defined by extrapolation to the present day, would be 10^{-21} G.

of the electron), takes on different values depending on the magnetic quantum number. It is through this magnetic moment that that the 21-cm emission is sensitive to ambient MFs, as explained in the following sections.

For unpolarized atoms, the detectability of the 21-cm signal hinges on the spin temperature T_s, which quantifies the relative number densities of atoms in the two hyperfine levels of the electronic ground state,

$$\frac{n(F=1)}{n(F=0)} = 3e^{-T_*/T_s}. \tag{1}$$

Here, $F = 0$ denotes the lower (spin-antiparallel) hyperfine level, $F = 1$ denotes the upper (spin-parallel) level, 3 is the ratio of statistical weights, and $T_* = \hbar\omega_{hf}/k_B = 68\,\mathrm{mK}$ is the hyperfine splitting in temperature units. A signal is detected if the spin temperature of the gas deviates from the temperature of the background CMB T_γ at that redshift; net emission occurs if $T_s > T_\gamma$ and absorption if $T_s < T_\gamma$. The spin temperature is determined by three major processes: (1) absorption/emission of 21-cm photons from/to the radio background at that redshift (primarily the CMB), (2) collisional excitation and de-excitation of hydrogen atoms, and (3) resonant scattering of Lyα photons from the first stars and galaxies, which can change the spin state via the spin-orbit interaction while the atom is in the excited state.

The fundamental quantity of interest observationally is the *brightness temperature* of the H I 21-cm line [42]. In the optically thin approximation, the brightness temperature *fluctuation* relative to the CMB at redshift z and hence observed at the frequency $\omega_{obs} = \omega_{hf}/(1 + z)$ is

$$\delta T_b \approx 27 x_{1s}(1+\delta)\frac{T_s - T_\gamma}{T_s}\left(\frac{1+z}{10}\right)^{1/2}\frac{(1+z)H(z)}{\partial_\parallel v_\parallel}\,\mathrm{mK} \tag{2}$$

(see e.g. Ref. [37]).[2] Here x_{1s} is the hydrogen neutral fraction (essentially all in the ground state), $1 + \delta$ is the matter density contrast, T_s is the spin temperature, and the line-of-sight velocity gradient $\partial_\parallel v_\parallel$ accounts for deviations from the expansion rate of the homogeneous universe.

In this paper, where we take account of the spin-polarization of atoms, we need to consider the full atomic density matrix, rather than T_s alone. We extend the formalism of 21-cm cosmology as needed to derive an equation for ΔT_b valid in this case. Several previous analyses have considered polarized 21-cm radiation from high redshift and its "scrambling" by Faraday rotation in passing through the interstellar medium of our own galaxy [43, 44]; however they did not study polarization of the emitting atoms[3], and thus did not need to develop the

formalism presented here.

B. Related methods: Hanle effect and ground-state alignment

The effect considered in this paper is closely related to the Hanle effect [45], which refers to the change in the polarization of resonant-scattering radiation in the presence of external MFs. In solar research, techniques based on the Hanle effect are used for measuring weak MFs in solar prominences and the upper solar atmosphere (see e.g. Refs. [46–52]). The methods of this paper use the irreducible tensor approach to the density matrix (see Ref. [53] for an overview and Ref. [48] for an application to the Hanle effect in solar physics).

The subject of this paper relies on atomic alignment, whose significance in the astrophysical context was first realized in the early days of maser studies. The theory of alignment in astrophysical environments was further developed in the pioneering work of Varshalovich [32, 33]. Other significant milestones were the work of Goldreich, Keeley and Kwan [54, 55], who considered the polarization of maser emission due to aligned molecules, and Goldreich and Kylafis [56], who proposed using linear polarization in radio lines as probes of magnetic fields in molecular clouds.

More recently, Yan & Lazarian [34–36] proposed a suite of methods to probe weak MFs in diffuse media using atomic alignment. Since the method discussed in this paper relies on the same atomic physics as these previous studies, we briefly summarize the main idea behind them. Their methods rely on the polarization and intensity of radiation interacting with atoms or ions with fine (or hyperfine) structure in the ground state. When these species are immersed in an anisotropic flux of photons, the orientation of the total atomic angular momentum vector gets a preferred direction since photons carry angular momentum and transfer it via interactions. If aligned atoms are further placed in an external MF, their orientations change due to Larmor precession. As a result, the output radiation's intensity and polarization changes in a manner depending on the direction and strength of the MF. The main advantage of using atomic species with (hyper)fine structure in their ground or metastable states is these states' long lifetimes. Longer lifetimes are associated with longer baselines for Larmor precession, which make the effect sensitive to very weak MFs. These authors recognize the relevance of this effect for studying magnetic fields during the EoR via the 21-cm line of neutral hydrogen [36] and the fine-structure lines of the first metals [57], but they do not include its calculation in the cosmological context.

The study in this paper distils elements from the physics of all the previous work on astrophysical alignment, and uses features unique to the study of the 21-cm line in the cosmological context in order to synthesize a new method for measuring MFs. In order

---

[2] Note that Eq. (7) in Ref. [37] is missing a -1 exponent.

[3] These works focused on polarization produced by re-scattering of 21-cm radiation by electrons in ionized regions. There is no anisotropy of the spins of the hydrogen atoms involved in that mechanism.
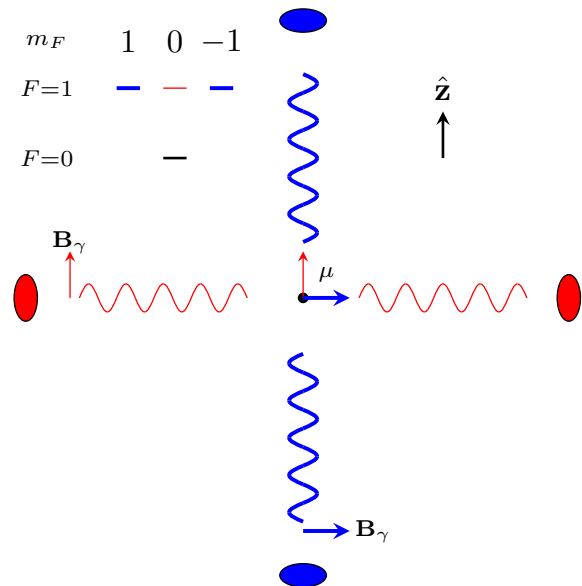
FIG. 1. An illustration of how an incident quadrupole spin-polarizes the triplet level of the hyperfine transition. The hydrogen atom (at the center) is surrounded by a quadrupole intensity pattern with hot (blue, thick lines) and cold (red, thin lines) spots. Absorption of 21-cm photons produces a state with a magnetic moment $\boldsymbol{\mu}$ aligned with the magnetic field $\boldsymbol{B}_\gamma$ of the incident radiation. The incident anisotropy is tranfered to the direction of the magnetic moment. **Inset:** The resulting unequal population of the triplet sublevels. For the orientation of this figure, the levels with magnetic quantum number $m_F = \pm 1$ (thick blue lines) are preferentially populated due to the hot spots.

to align the excited state of the 21-cm transition, our method relies on 'resonant' anisotropies (at frequencies $\nu = 1.42$ GHz) that are sourced by fluctuations of Large Scale Structure (LSS). This is closely related to the mechanism of Refs. [54–56], in that it uses anisotropies in optical depth sourced by velocity gradients in order to achieve alignment. The mechanism studied in [34–36] aligns the triplet via optical pumping by anisotropies in the incident Lyman-α radiation field, i.e. at frequencies $\nu \approx 2.46 \times 10^{15}$ GHz.

Our method also differs from these previous methods in the respect that it uses relatively subtle changes in the intensity of the outgoing radiation to detect MFs. Refs. [34–36] recognize the change in the net emissivity, and propose using the emissivity ratio of multiple lines to probe MFs. As we show in this paper, it is possible to use *solely* the 21cm transition, due to the statistical nature of its measurement in cosmology. The cosmic density field contains perturbation modes with a variety of wave vectors $\boldsymbol{k}$, whose amplitudes obey the underlying statistical isotropy of the Universe. The anisotropy in the scattering properties caused by the MF can then be probed using the varying illumination conditions (depending on the direction of $\hat{\boldsymbol{k}}$), rather than the polarization of outgoing radiation.

III. ILLUSTRATION AND SIMPLE ESTIMATE OF THE EFFECT

Consider a hydrogen atom in the ground state of the hyperfine transition, located in the overdense part of a growing Fourier mode at a suitably high redshift. Moreover, let us assume that the 21-cm line is visible in emission. The brightness temperature fluctuation $\delta T_{\rm b}$ seen by this atom along a particular line of sight (LOS) $\hat{\boldsymbol{n}}$ is largely due to stimulated emission and absorption by a thermal background of excited atoms, and is proportional to the optical depth τ integrated along that direction,

$$\delta T_{\rm b}(\hat{\boldsymbol{n}}) \approx \tau(\hat{\boldsymbol{n}})(T_{\rm s} - T_\gamma), \tag{3}$$

where $T_{\rm s}$ and T_γ are the spin- and CMB-temperatures, respectively.

The optical depth, in turn, depends on the path length over which photons stay within the line:

$$\tau(\hat{\boldsymbol{n}}) \sim n \int \sigma(\nu){\rm d}l = n \int \sigma(\nu)\frac{{\rm d}l}{{\rm d}\nu}{\rm d}\nu \sim \frac{n\sigma(\nu_0)c\Delta}{{\rm d}v_{||}/{\rm d}r_{||}(\hat{\boldsymbol{n}})}, \tag{4}$$

where $\sigma(\nu)$ is the absorption cross-section at frequency ν, ν_0 is the frequency at line-center, Δ is the dimensionless Doppler width of the line, c is the speed of light, and ${\rm d}v_{||}/{\rm d}r_{||}(\hat{\boldsymbol{n}})$ is the velocity gradient along the LOS. The velocity gradient term equals the Hubble rate when the LOS is orthogonal to the wave-vector $\boldsymbol{k}$ of the Fourier mode, but it picks up a contribution from the infall into the growing overdensity when the LOS has a component

along $\boldsymbol{k}$. For an arbitrary direction of the LOS, the velocity gradient term equals

$$\frac{{\rm d}v_{||}}{{\rm d}r_{||}}(\hat{\boldsymbol{n}}) = H + \frac{{\rm d}v_{\rm infall,||}}{{\rm d}r_{||}}(\hat{\boldsymbol{n}}) = H\left[1 - (\hat{\boldsymbol{k}}\cdot\hat{\boldsymbol{n}})^2\delta\right]. \tag{5}$$

Hence the optical depth of the medium around the atom has a quadrupole dependence with a fractional size proportional to the overdensity, or an absolute size of $\mathcal{O}(\delta\tau)$. This leads to a quadrupole in the incident brightness temperature, oriented such that directions along the wave-vector are hotter.

Atoms that are excited by absorption have magnetic moments that are aligned with the exciting radiation's magnetic field. For anisotropic incident radiation, this leads to a preference for directions orthogonal to that of hot spots in the incident radiation field. Thus an incident quadrupole spin-polarizes the atoms, i.e. unequally populates the states within the hyperfine triplet. Figure 1 illustrates this effect.

These excited atoms de-excite to the ground state mainly by stimulated emission or non-radiative processes. The former leads to an output quadrupole pattern with the same orientation as the incident one, but a smaller size of $\mathcal{O}(\tau\,\delta\tau)$. This is illustrated in Fig. 2.

field along the $z-$axis, the solution is

$$\boldsymbol{\mu}(t) = e^{-t/t_{\mathrm{d}}} \begin{pmatrix} \cos\left(\omega_{\mathrm{L}}t\right) & -\sin\left(\omega_{\mathrm{L}}t\right) & 0 \\ \sin\left(\omega_{\mathrm{L}}t\right) & \cos\left(\omega_{\mathrm{L}}t\right) & 0 \\ 0 & 0 & 1 \end{pmatrix} \boldsymbol{\mu}_0. \quad (7)$$

Thus the moment precesses through an angle $\theta_{\mathrm{B}} \approx \omega_{\mathrm{L}}t_{\mathrm{d}}$ before the atom de-excites. If the de-excitation occurs only via radiative processes, the lifetime is

$$t_{\mathrm{d}}^{-1} \approx A \frac{k_{\mathrm{B}}T_{\gamma}}{\Delta E_{\mathrm{hf}}}, \quad (8)$$

where k_{B} is the Boltzmann constant, ΔE_{hf} is the hyperfine energy gap, and A is the Einstein A-coefficient or intrinsic width of the line, which is broadened due to stimulated emission by the background CMB with a temperature T_{γ}.

We estimate the angle of precession to be

$$\theta_{\mathrm{B}} \approx \omega_{\mathrm{L}}t_{\mathrm{d}} = \frac{\gamma_{\mathrm{e}}\Delta E_{\mathrm{hf}}}{Ak_{\mathrm{B}}T_{\gamma}}B = 1.5 \times \left(\frac{B}{10^{-19}\mathrm{G}}\right)\left(\frac{1+z}{10}\right)^{-1}, \quad (9)$$

where γ_{e} is the gyromagnetic ratio of the electron. Figure 2 illustrates the precession of the magnetic moment, and that of the quadrupole associated with the secondary emission. If the background magnetic field varies on larger scales than that of the fluctuations in the 21–cm signal, it is effectively homogenous over the length-scale of the modes of interest. In this case, we see from the geometry of the figure (with the magnetic field along the $z-$axis) that the change in a mode's brightness temperature depends on which quadrant of the $x-y$ plane the projection of $\boldsymbol{k}$ lies in. Keeping the line of sight along $\hat{\boldsymbol{y}}$ and assuming the precession angle is small,

$$\delta T_{\mathrm{b}}|_{\mathrm{pr}} \sim (T_{\mathrm{s}} - T_{\gamma})\tau\,\delta\tau\left(\theta_{\mathrm{B}_{\mathrm{z}}}\hat{\boldsymbol{k}}_x\hat{\boldsymbol{k}}_y - \theta_{\mathrm{B}_{\mathrm{x}}}\hat{\boldsymbol{k}}_y\hat{\boldsymbol{k}}_z\right). \quad (10)$$

The precession-induced correction shown in Eq. (10) distorts the angular structure of the 21-cm emission in a manner unlike any of the usually considered effects – it breaks the symmetry around the line of sight. This distinguishes it from corrections like the usual redshift space distortions due to peculiar velocities. Fig. 3 illustrates this.

In the rest of the paper we go beyond this simple semi-classical treatment of the spin-polarization, and compute the rates of de-polarization by other non-radiative channels.

IV.   NOTATION AND BASIC FORMALISM

Table I lists the symbols used throughout this paper and the physical quantities they represent.

A.   Atomic Density Matrix

We study the level populations of the hydrogen ground state using the density matrix formalism [58]. If we con-
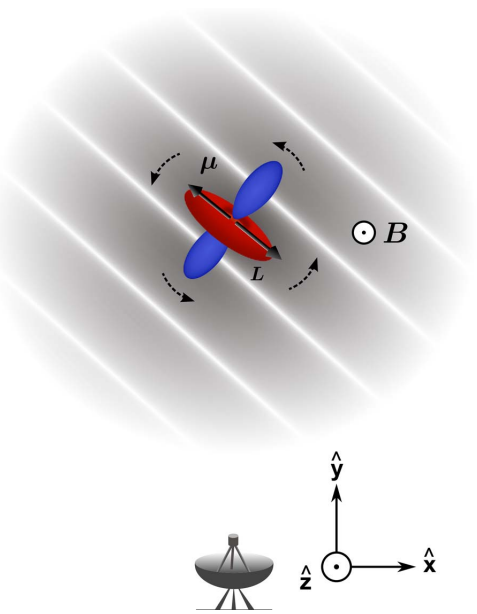

FIG. 2. A hydrogen atom in a growing plane wave density fluctuation: The atom is excited to the spin-polarized state of Fig. 1, which produces the quadrupolar radiation pattern shown above when it de-excites. Also shown is one possible orientation of the intermediate magnetic moment $\boldsymbol{\mu}$, and the associated angular momentum $\boldsymbol{L}$. If an external magnetic field $\boldsymbol{B}$ is present, the torque it exerts ($\boldsymbol{\mu} \times \boldsymbol{B}$) causes the moment to precess around it before it de-excites. If the field is coherent on larger scales than the fluctuations in the 21–cm signal (and thus homogenous on the latter's scales), and has a component in the plane of the observer's sky, it systematically changes the brightness temperature for a plane wave as a function of the latter's orientation.

The angular structure of the observed brightness temperature fluctuations is dominated by the contribution of the pre-existing thermal background of excited atoms, and is $\mathcal{O}(\delta\tau)$ in size, as can be seen from Eq. (3). The secondary emission described above is much smaller (by a factor of the optical depth, τ), and does not correspond to a qualitatively different pattern.

The presence of a homogenous background magnetic field breaks isotropy and leads to a unique signature in the angular pattern of this secondary emission. To see this, consider the effect of a magnetic field on the intermediate magnetic moment, which has a finite lifetime t_{d}. This lifetime is mainly due to stimulated emission and non-radiative processes such as collisions and optical pumping by Lyman-α photons. Additionally, the moment precesses about the background magnetic field $\boldsymbol{B}$ with the Larmor frequency ω_{L}.

Due to these effects, the moment $\boldsymbol{\mu}$ evolves as

$$\frac{\mathrm{d}}{\mathrm{d}t}\boldsymbol{\mu} \approx -\frac{\boldsymbol{\mu}}{t_{\mathrm{d}}} - \omega_{\mathrm{L}}\boldsymbol{\mu} \times \widehat{\boldsymbol{B}}. \quad (6)$$

In a coordinate system with the background magnetic

TABLE I. Glossary of symbols used in this paper.

Symbol	Physical quantity
ρ	Density matrix of neutral hydrogen atoms
ρ_{aa}	Singlet state sub-matrix of ρ. It is a scalar which corresponds to the occupancy of the singlet state
ρ_{mn}	Triplet state sub-matrix of ρ
$\mathscr{P}_{jm}$	Irreducible components of ρ_{mn}
ω_{hf}	Angular frequency of the hyperfine transition
T_*	Hyperfine gap expressed in temperature units
A	Einstein A-cofficient for the hyperfine transition
$k^{\pm}$	Averaged cross-sections for collisional transitions
$\kappa(1\text{-}0)$	Collisional rate for transition from triplet to singlet state
$\kappa(0\text{-}1)$	Collisional rate for transition from singlet to triplet state
$\kappa^{(j)}(1\text{-}0)$	Collisional depolarization rates for rank-j irreducible components
n	Principal quantum number
l	Azimuthal quantum number
m	Magnetic quantum number
F	Total angular momentum (nuclear + electronic)
m_F	Total magnetic quantum number
J_α	Flux of Lyman-α photons on the blue side of the line (in $\mathrm{cm}^{-2}\mathrm{s}^{-1}\mathrm{Hz}^{-1}\mathrm{sr}^{-1}$)
$T_{\mathrm{c,eff}}$	Effective color temperature in the vicinity of the Lyman-α resonance
$\Gamma_{2\mathrm{p}}$	Einstein A-coefficient for the Lyman-α transition
$\gamma_{2\mathrm{p}}$	$= \Gamma_{2\mathrm{p}}/4\pi$, HWHM of the Lyman-$\alpha$ transition
$\phi_{\mathrm{AB}}(\nu)$	Interference profiles for the lines A and B
$\sigma_{F_I \to F_J,(j)}(\nu)$	Cross section for the transition between the rank-j components of multiplets with $F = F_I, F_J$ due to optical pumping by incident Lyman-α photons of frequency ν
$\tilde{S}_\alpha, \tilde{S}_{\alpha,(2)}$	Correction factors for the detailed frequency dependence of Lyman-α flux, entering the rate equations for $\mathscr{P}_{00}$ and $\mathscr{P}_{2m}$
$\boldsymbol{k}_\gamma$	Wave-vector of the radiation
$\hat{\boldsymbol{n}}$	Direction of the radiation's propagation (line-of-sight from the emitter to the observer)
$f_{\alpha\beta}(\omega)$	Phase space density (p.s.d) matrix for the radiation
$f_X(\omega)$	Parity invariants of the radiation's p.s.d
$\mathcal{F}_{jm}(\omega)$	Irreducible components of the radiation's p.s.d
$\phi(\omega)$	Absorption profile for the hyperfine transition
$\mathcal{X}(\omega)$	Cumulative function for $\phi(\omega)$
$\sigma(\omega)$	Absorption cross-section for the hyperfine transition
τ	Optical depth of the medium
δT_{b}	Brightness temperature fluctuation of the 21-cm line relative to the CMB
$x_{\alpha,(2)}$	Relative strength of depolarization through optical pumping and radiative channels
$x_{\mathrm{c},(2)}$	Relative strength of depolarization through collisions and radiative channels
x_{B}	Relative rates of precession and radiative depolarization
δ	Local overdensity
$\boldsymbol{v}$	Bulk matter velocity
$\boldsymbol{k}$	Wave-vector of the growing mode of the matter density
z	Redshift
T_{s}	Spin temperature
T_γ	CMB temperature
T_{k}	Kinetic temperature
n_{H}	Number density of hydrogen atoms
$x_{1\mathrm{s}}$	Fraction of hydrogen atoms in the 1s state
H	Hubble expansion rate
$\boldsymbol{B}$	External magnetic field in the region of interest

sider an ensemble of atoms consisting of a mixture of states $|\psi_\alpha\rangle$ with statistical weights W_α, then the density operator is defined as $\rho = \sum_\alpha W_\alpha |\psi_\alpha\rangle\langle\psi_\alpha|$. In order to express the density operator in matrix form, we choose a set of basis states $|\phi_I\rangle$; the matrix elements of ρ are then

given by

$$\rho_{IJ} = \langle|\phi_J\rangle\langle\phi_I|\rangle = \sum_\alpha W_\alpha \langle\phi_I|\psi_\alpha\rangle\langle\psi_\alpha|\phi_J\rangle. \qquad (11)$$

The interaction between the electronic and the nuclear spin splits the ground state of the hydrogen atom into a superposition of two hyperfine levels, a singlet with quantum numbers $(F = 0, m_F = 0)$, and a triplet with
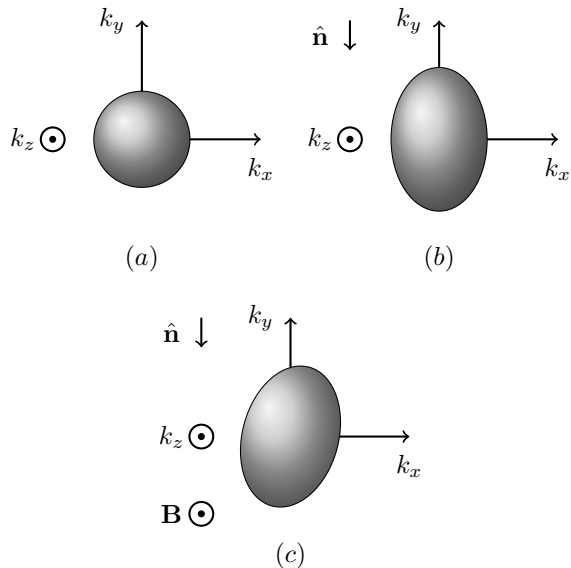
FIG. 3. This figure illustrates the effect on the power-spectrum of the brightness temperature fluctuations. The sub-figures show contours of constant power in $\boldsymbol{k}$-space. (a) Fluctuations of the 21-cm emissivity (photons per cm^3 per s emitted over all solid angles) in the rest-frame of the emitting atoms. (b) Fluctuations as seen by a distant (present-day) observer. Note the elongation in the direction of the line of sight to the observer, $\hat{\boldsymbol{n}}$, due to peculiar velocities. This manifests as a "compression" in the real-space correlation function, but as a power enhancement ("stretching" of the $P(\boldsymbol{k})$ contours) in Fourier-space. (c) Fluctuations with an external magnetic field added. The effect of the precession is to break the symmetry around $\hat{\boldsymbol{n}}$. The size of the effects has been exaggerated in (b) and (c).

$(F = 1, m_F = 0, \pm 1)$. As long as we consider the subset of neutral hydrogen atoms in the 1s electronic state, these states form a complete basis. In the ket notation, these states are represented by $|Fm_F\rangle$.

We will henceforth adopt the convention that indices of the kind $I, J, \ldots$, when used as subscripts for the density matrix ρ or as state labels, run over all four of the hyperfine states of the 1s type. They are purely abstract indices. Depending on the context, their instantiations are either the lower-case roman letters $a, b, c,$ and d or the numbers 1, 0, and -1. Table II maps the various indices to states. Note that numerical subscripts, referred to by $m, n, \ldots$ in the text, run over only the triplet states. They equal the magnetic quantum numbers of the respective states. Thus summations over these numeric indices represent ones over only the triplet states.

Within the basis of the two hyperfine levels, the density matrix is of the form

$$\rho = \rho_{IJ} = \begin{pmatrix} \overbrace{\rho_{aa}}^{1 \times 1} & \rho_{am} \\ \rho_{ma} & \underbrace{\rho_{mn}}_{3 \times 3} \end{pmatrix}. \tag{12}$$

This density matrix consists of four submatrices. The upper diagonal submatrix has only one element (ρ_{aa}) that describes the probability of finding an atom in the singlet state. The lower diagonal submatrix describes the triplet state. Its diagonal elements represent the probabilities of finding atoms with $F = 1$ in the states with the corresponding quantum number m_F. The off-diagonal elements describe coherences between states of different m_F. The remaining two submatrices, with elements in the first row or column describe the interference between $F = 0$ and $F = 1$ levels. The time evolution of these terms is proportional to $\exp(i\omega_{\rm hf}t)$, where $\omega_{\rm hf} = 2\pi \times 1420$ MHz is the angular frequency corresponding to the hyperfine gap. These terms rapidly oscillate on macroscopic timescales with average values of zero, thus we do not need to follow them in the calculation.

The processes we are interested in only redistribute atoms between the levels, hence the trace of the density matrix is preserved by them. The trace can be taken to be unity as long as we are interested in the population of atoms in the ground electronic state i.e. $\rho_{aa} + \text{Tr}(\rho_{mn}) = 1$.

The 4×4 Hermitian matrix ρ is described by sixteen real numbers. Removing the six real degrees of freedom constituting the sub-matrix ρ_{am}, and the singlet sub-matrix ρ_{aa}, leaves nine real numbers describing the triplet state sub-matrix ρ_{mn}.

In order to take advantage of the symmetries of the problem, it is convenient to express the density matrix in terms of irreducible tensor operators. We construct irreducible components of ranks $j = \{0, 1, 2\}$ from the elements of the triplet sub-matrix, in the manner of Ref. [59]: [4]

$$\mathscr{P}_{jm} = \sqrt{3(2j+1)} \sum_{m_1,m_2} (-1)^{1-m_2} \begin{pmatrix} 1 & j & 1 \\ -m_2 & m & m_1 \end{pmatrix} \times \rho_{m_1 m_2}, \tag{13}$$

where the expression in large parentheses is the Wigner 3-j symbol. The indices j and m indicate that the irreducible component $\mathscr{P}_{jm}$ transforms in the same way as the corresponding spherical harmonic Y_{jm} does under a rotation of the axes – only components with the same rank j mix. The Hermiticity of the density matrix leads to the characteristic behavior of these components under complex conjugation:

$$\mathscr{P}_{j-m} = (-1)^m \mathscr{P}_{jm}^*. \tag{14}$$

The components of rank zero, one and two are described by one, three and five real numbers respectively. As expected, both descriptions of the triplet state density sub-matrix have the same total number of real degrees of freedom.

———

[4] Note that the definition in Ref. [59] differs from ours by a factor of i^j, due to their usage of a different convention for spherical tensors.

TABLE II. Notation for hyperfine states.

$|F m_F\rangle$	Roman	Numeric
$|0\ 0\rangle$	a	-
$|1\ -1\rangle$	b	-1
$|1\ 0\rangle$	c	0
$|1\ 1\rangle$	d	1

We recover the density matrix in the standard basis from the irreducible components using the following relation:

$$\rho_{m_1 m_2} = \sum_{jm} \sqrt{\frac{2j+1}{3}} (-1)^{1-m_2} \begin{pmatrix} 1 & j & 1 \\ -m_2 & m & m_1 \end{pmatrix} \mathscr{P}_{jm}. \tag{15}$$

The operator of rank zero is a scalar representing the net probability of finding an atom in the triplet, or $F = 1$, state.: $\mathscr{P}_{00} = \mathrm{Tr}(\rho_{mn})$. The operator of rank one is a vector with three components, and is often called the *orientation vector*. It is proportional to the internal angular momentum of the ensemble. The operator of rank two is the so-called *alignment tensor*, which has five components that are quadratic in angular momentum and has the symmetry of an electric quadrupole.

In many applications, excitations between the singlet and the triplet are isotropic. In such cases, only the operator of rank zero, or the net excited-state occupancy, is relevant. The scenario of interest in this paper involves anisotropic excitations, thus we need to use operators of higher rank to describe the spin state of the atoms, which are said to be *spin-polarized*.

For a system in equilibrium with a heat bath with temperature T, the elements of the density matrix take the form

$$\rho_{IJ}^{\mathrm{th}} = \frac{e^{-\beta E_I}}{Z} \delta_{IJ}, \tag{16}$$

where $\beta = (k_B T)^{-1}$, and $Z = \sum_I e^{-\beta E_I}$ is the partition function of the ensemble.

Given a general density matrix ρ_{IJ}, the spin temperature T_s is defined using this equilibrium formula:

$$\frac{\mathscr{P}_{00}}{1 - \mathscr{P}_{00}} = \frac{\rho_{11} + \rho_{00} + \rho_{-1-1}}{\rho_{aa}} = 3 e^{-(\hbar \omega_{\mathrm{hf}}/k_B T_s)}. \tag{17}$$

In the regimes of interest, the spin temperature is much larger than the temperature associated with the gap, which is $T_* = \hbar \omega_{\mathrm{hf}}/k_B = 68.2$ mK. In this limit, the occupancy of the excited state is

$$\mathscr{P}_{00} \approx \frac{3}{4} - \frac{3 T_*}{16 T_s}. \tag{18}$$

B. Phase-space density matrix for radiation

In this section and subsequent sections, we use the Coulomb gauge to describe the electromagnetic field, in which $\nabla \cdot \boldsymbol{A} = 0$ and there is no scalar potential associated with the radiation. The phase space distribution of the radiation and its multipole decomposition – including the description of the linear polarization in "E" and "B" modes – follows the development in the CMB literature [60, 61].

As long as we can approximate the electromagnetic field as Gaussian, we can describe its general state by a density matrix, in the same manner as the spin-states of the hydrogen atoms in Section IV A. We explicitly realize this by expanding the vector potential in the plane-wave basis:

$$\boldsymbol{A}(\boldsymbol{r}) = \sum_{\boldsymbol{k}_\gamma, \alpha} \left[a_\alpha(\boldsymbol{k}_\gamma) \boldsymbol{A}_{\boldsymbol{k}_\gamma, \alpha}(\boldsymbol{r}) + a_\alpha^\dagger(\boldsymbol{k}_\gamma) \boldsymbol{A}_{\boldsymbol{k}_\gamma, \alpha}^*(\boldsymbol{r}) \right], \tag{19}$$

with mode functions given by

$$\boldsymbol{A}_{\boldsymbol{k}_\gamma, \alpha}(\boldsymbol{r}) = \left(\frac{2\pi \hbar c^2}{\omega} \right)^{1/2} \boldsymbol{e}_{(\alpha)}(\hat{\boldsymbol{k}}_\gamma) e^{i \boldsymbol{k}_\gamma \cdot \boldsymbol{r}} , \quad \alpha = \pm, \tag{20}$$

where $\boldsymbol{k}_\gamma$ is the radiation's wave-vector. The subscript on the wave-vector distinguishes it from that of the density fluctuations. The summation over $\boldsymbol{k}_\gamma$ is shorthand for the integral $\int d^3 \boldsymbol{k}_\gamma / (2\pi)^3$, and the angular frequency is given by $\omega = c k_\gamma$. The symbol $\boldsymbol{e}_{(\pm)}(\hat{\boldsymbol{k}}_\gamma)$ represents right- and left-circularly polarized states, respectively. In terms of the unit vectors $\hat{\boldsymbol{\theta}}$ (north-south polarization) and $\hat{\boldsymbol{\phi}}$ (east-west polarization):

$$\boldsymbol{e}_{(\pm 1)}(\hat{\boldsymbol{k}}_\gamma) = \mp \frac{1}{\sqrt{2}} (\hat{\boldsymbol{\theta}} \pm i \hat{\boldsymbol{\phi}})|_{(\theta, \phi) = (\theta_{k_\gamma}, \phi_{k_\gamma})} . \tag{21}$$

The expansion coefficients in Eq. (19) are annihilation and creation operators for photons with momentum $\hbar \boldsymbol{k}_\gamma$, with canonical commutation relations.

We define the density matrix for radiation in a manner almost exactly paralleling that of Eq. (11), which defined it for the atoms:

$$\langle a_\alpha^\dagger(\boldsymbol{k}_\gamma) a_\beta(\boldsymbol{k}_\gamma') \rangle = (2\pi)^3 \delta(\boldsymbol{k}_\gamma - \boldsymbol{k}_\gamma') f_{\beta\alpha}(\omega, \hat{\boldsymbol{n}} = \hat{\boldsymbol{k}}_\gamma), \tag{22}$$

where $\hat{\boldsymbol{n}}$ denotes the direction of propagation. In the general polarized case, the phase-space density matrix for the photons, $f_{\alpha\beta}(\omega, \hat{\boldsymbol{n}})$, is of the form:

$$f_{\alpha\beta} = \begin{pmatrix} f_{++} & f_{+-} \\ f_{-+} & f_{--} \end{pmatrix} = \begin{pmatrix} f_{\mathrm{I}} + f_{\mathrm{V}} & -f_{\mathrm{Q}} + i f_{\mathrm{U}} \\ -f_{\mathrm{Q}} - i f_{\mathrm{U}} & f_{\mathrm{I}} - f_{\mathrm{V}} \end{pmatrix}. \tag{23}$$

The decomposition of the phase-space density matrix in Eq. (23) connects it to the Stokes parameters:

$$X(\omega, \hat{\boldsymbol{n}}) = \frac{\hbar}{c^2} \frac{\omega^3}{4\pi^3} f_X(\omega, \hat{\boldsymbol{n}}), \qquad X \in \{\mathrm{I}, \mathrm{Q}, \mathrm{U}, \mathrm{V}\}, \tag{24}$$

where the quantities are defined per unit angular frequency ω.

The elements of the phase-space density matrix transform differently under a rotation of the axes. The diagonal elements are scalars, while the off-diagonal elements

are quantities with spin weights of ± 2 [62]. Hence, they are decomposed into moments as follows:

$$f_{\alpha\beta}(\omega, \hat{\boldsymbol{n}}) = \sum_{j,m} \sqrt{\frac{4\pi}{2j+1}} (f_{\alpha\beta})_{jm}(\omega) \left[{}_{\alpha-\beta}Y_{jm}(\hat{\boldsymbol{n}}) \right]^*. \tag{25}$$

The quantity ${}_sY_{jm}(\hat{\boldsymbol{n}})$ is the spin-weighted spherical harmonic with spin-weight s. The convention of Eq. (25) is slightly different from that in the standard cosmology literature. Appendix A expands on the difference and the reason for adopting the current convention.

Inversion of the coordinate axes (a parity transformation) transforms quantities with spin weights of ± 2 into each other. We further split the moments into parity invariants as follows:

$$(f_{++/--})_{jm} = f_{\mathrm{I},jm} \pm f_{\mathrm{V},jm}, \tag{26a}$$

$$(f_{+-/-+})_{jm} = -f_{\mathrm{E},jm} \pm i f_{\mathrm{B},jm}. \tag{26b}$$

The quantities $f_{\mathrm{I},jm}$ and $f_{\mathrm{V},jm}$ are moments of the intensity and circular polarization respectively. A parity transformation multiplies the quantities $f_{\mathrm{E},jm}$ and $f_{\mathrm{B},jm}$ by factors of $(-1)^j$ and $(-1)^{j+1}$ respectively.

In this section, we used the plane wave basis to define the phase-space density matrix and its moments. The interaction term between the atoms and radiation is particularly simple when the EM field is expressed in the spherical wave basis [48]. Hence we use this basis in the calculation of the evolution of the atomic density matrix due to interaction with radiation.

Appendix B expands on the details of the spherical wave basis, and the steps involved in moving back and forth between it and the plane wave basis.

V. INTERACTION BETWEEN HYDROGEN ATOMS AND 21-CM RADIATION

In this section, we work out the effect of radiative transitions to and from spin-polarized states of the hydrogen atom. We generalize the usual treatment of absorption, and spontaneous and stimulated emission from the level occupancies to the full density matrix ρ. Our description of the atom-radiation interaction Hamiltonian is similar, in principle if not in detail, to Sections 14.1 and 15.4 of Mandel & Wolf [63].

The dominant interaction is via a magnetic dipole, and involves the emission or absorption of $j=1$ photons of the magnetic type. The transition matrix element between an initial state I, and a final state J, is [59]

$$V_{JI,m}(\omega) = -i\sqrt{\frac{2}{3\pi}} \left(\frac{\hbar\omega^3}{c^3} \right)^{1/2} \left[-e\{Q_{1,m}^{(M)}\}_{JI} \right], \tag{27}$$

where the angular frequency ω and the magnetic quantum number m describe the photon absorbed in the process, and $\{Q_{1m}^{(M)}\}_{JI}$ is a spherical component of the magnetic dipole moment $\boldsymbol{Q}_{JI}^{(M)}$. The magnetic dipole moment

is related to the electron's spin-angular momentum by the gyromagnetic ratio i.e. $-e\,\boldsymbol{Q}^{(M)} = -(g_{\mathrm{e}}\mu_{\mathrm{B}}/\hbar)\boldsymbol{S}_{\mathrm{e}}$, where g_{e} is the Landé g-factor for the electron spin and μ_{B} is the Bohr magneton.

The initial state is the singlet state a, the final state lies within the triplet, and the index m is fixed by angular momentum conservation. In order to make this clearer, we substitute these states in Eq. (27) and rewrite it in the form

$$V_{m_F a,m}(\omega_{\mathrm{hf}}) = i\hbar \sqrt{\frac{A}{2\pi}} \delta_{mm_F}, \tag{28}$$

where $A = 2.86 \times 10^{-15}\,\mathrm{s}^{-1}$ is the Einstein coefficient for the hyperfine transition.

Given the transition matrix element, the atom-radiation interaction Hamiltonian is[5]

$$H_{\mathrm{hf},\gamma} = \sum_{m_F m} \int d\omega \, V_{m_F a,m}(\omega) |1m_F\rangle\langle 00| a_{1m}^{(M)}(\omega) + \mathrm{h.c.} \tag{29}$$

Here "h.c." stands for the Hermitian conjugate. The quantity $a_{1m}^{(M)}(\omega)$ is an annihilation operator for a photon of the magnetic type, expanded upon in Appendix B.

From here onwards, we use a dot over a quantity to represent its time evolution. Equation (11) enables us to write down the evolution of the triplet state sub-matrix ρ_{mn} due to the interaction with the EM field. The underlying operator commutes with the matter Hamiltonian, so its evolution is solely due to the interaction $H_{\mathrm{hf},\gamma}$, specifically:

$$\dot{\rho}_{m_1 m_2}|_\gamma$$
$$= \frac{i}{\hbar} \langle [H_{\mathrm{hf},\gamma}, |1m_2\rangle\langle 1m_1|] \rangle$$
$$= \frac{i}{\hbar} \sum_m \int d\omega V_{m_2 a,m}^*(\omega) \left\langle |00\rangle\langle 1m_1| a_{1m}^{(M)\dagger}(\omega) \right\rangle + \mathrm{c.c.s.} \tag{30}$$

Here "c.c.s." stands for complex conjugation with a swap (i.e. swap $m_1 \leftrightarrow m_2$).

The three-point functions of the atom and the radiation field represent transitions between the singlet and the triplet levels. Appendix C derives expressions for such three-point functions. Plugging in Eq. (C5) gives the evolution equation

$$\dot{\rho}_{m_1 m_2}|_\gamma = -\frac{\pi}{\hbar^2} \sum_{m,m',m_3} V_{m_2 a,m}^* V_{m_3 a,m'}$$
$$\times \left[\rho_{m_1 m_3} \left\{ \delta_{mm'} + f_{m',m}^{(M1)(M1)} \right\} \right.$$
$$\left. - \delta_{m_3 m_1} \rho_{aa} f_{m',m}^{(M1)(M1)} \right] + \mathrm{c.c.s.} \tag{31}$$

This uses the notation for the radiation's phase-space density matrix in the spherical basis, defined in Eq. (B6) of Appendix B. The transition matrix elements and phase-space density moments are evaluated at $\omega_{\rm hf}$, the angular frequency of the hyperfine transition. However, the frequency in the bulk-rest frame corresponding to $\omega_{\rm hf}$ in the interacting atoms' frame is distributed over a broadened profile due to the thermal motions of the atoms.

In this calculation, we assume that the atom density matrix is independent of the velocity. The practical consequence of this assumption is that Eq. (31) can be used as is, with the radiation's phase space density averaged over a Doppler-broadened profile centered around $\omega_{\rm hf}$. The consequences of relaxing this assumption have been explored in a different context before [64]. In subsequent equations, a bar over quantities is used to indicate averages over the line profile.

In order to simplify the evolution given by Eq. (31), it is convenient to divide the terms into spontaneous and stimulated emission, and photo-absorption contributions.

Spontaneous emission is described by the terms in Eq. (31) connecting the excited state density sub-matrix ρ_{mn} to itself. We write these terms in terms of the irreducible components $\mathscr{P}_{jm}$ using Eqs. (13) and (15):

$$\dot{\mathscr{P}}_{jm}|_{\rm sp.em} = -A\mathscr{P}_{jm}. \tag{32}$$

Absorption is described by the terms in Eq. (31) connecting the excited state density sub-matrix ρ_{mn} to the ground state occupancy ρ_{aa}. Using Eq. (28), we write this contribution as

$$\dot{\rho}_{m_1 m_2}|_{\rm ab} = A \, \rho_{aa} \, \overline{f^{(M1)(M1)}_{m_1,m_2}}. \tag{33}$$

We can define irreducible components, $\mathcal{F}_{jm}$, of the M1–M1 block of the photon phase-space density matrix in the same manner as those of the triplet state density sub-matrix [see Eq. (B10)]. The photo absorption contribution retains its form when expressed in terms of the irreducible components:

$$\dot{\mathscr{P}}_{jm}|_{\rm ab} = A \, \rho_{aa} \, \overline{\mathcal{F}_{jm}} = A \, (1 - \mathscr{P}_{00}) \, \overline{\mathcal{F}_{jm}}. \tag{34}$$

Stimulated emission is described by the terms in Eq. (31) connecting the excited state density sub-matrix ρ_{mn} to itself, via the photon phase-space density moments $f^{(M1)(M1)}_{m,n}$. Using Eq. (28), this contribution is

$$\dot{\rho}_{m_1 m_2}|_{\rm st.em} = -\frac{A}{2} \sum_{m_3} \rho_{m_1 m_3} f^{(M1)(M1)}_{m_3,m_2} + {\rm c.c.s.} \tag{35}$$

Using Eqs. (13), (15) and (B11), we rewrite this in terms of the irreducible components $\mathscr{P}_{jm}$ and $\mathcal{F}_{jm}$:

$$\dot{\mathscr{P}}_{jm}|_{\rm st.em}$$
$$= -\frac{A}{2} \sum_{m_1 m_2 m_3} \sum_{j'm'j''m''} \sqrt{\frac{(2j+1)(2j'+1)(2j''+1)}{3}}$$

$$\times (-1)^{1-m_3} \left[\begin{pmatrix} 1 & j & 1 \\ -m_2 & m & m_1 \end{pmatrix} \begin{pmatrix} 1 & j' & 1 \\ -m_3 & m' & m_1 \end{pmatrix} \right.$$
$$\left. \times \begin{pmatrix} 1 & j'' & 1 \\ -m_2 & m'' & m_3 \end{pmatrix} + (j'm' \leftrightarrow j''m'') \right] \mathscr{P}_{j'm'} \overline{\mathcal{F}_{j''m''}}. \tag{36}$$

The summations over angular indices for products of three 3-j symbols, when evaluated, yield the product of a Wigner 6-j symbol along with a 3-j symbol [65]. Thus the evolution of the irreducible components $\mathscr{P}_{jm}$ due to stimulated emission is

$$\dot{\mathscr{P}}_{jm}|_{\rm st.em} = -A \sum_{j',j''} \sqrt{\frac{(2j'+1)(2j''+1)}{3}} \begin{Bmatrix} j'' & j' & j \\ 1 & 1 & 1 \end{Bmatrix}$$
$$\times \left[\frac{(-1)^j + (-1)^{j''-j'}}{2} \right] (\mathscr{P}_{j'} \otimes \overline{\mathcal{F}_{j''}})_{jm}. \tag{37}$$

The expression enclosed in curly braces is the 6-j symbol, and the notation $(\mathscr{P}_{j_1} \otimes \mathcal{F}_{j_2})_{jm}$ denotes the sum of products of the irreducible quantities $\mathscr{P}_{j_1 m_1}$ and $\mathcal{F}_{j_2 m_2}$, weighted with appropriate 3-j symbols, to yield a quantity which transforms in the (jm) representation.

In the absence of a density fluctuation, the excited states are isotropically occupied. Thus only the irreducible moment $\mathscr{P}_{00}$ has a zeroth-order contribution. The radiation field is unpolarized in this case, so only the intensity monopole has a zeroth-order contribution. Thus the only relevant radiation moment in the unperturbed case is $\mathcal{F}_{00}$.

As discussed in Section III, a growing density fluctuation leads to an incident quadrupole on the atoms. Hence the extra radiation moment exciting the atoms is of the $\mathcal{F}_{2m}$ type. The spin-polarization due to this quadrupole is described by the alignment tensor $\mathscr{P}_{2m}$. The orientation tensor $\mathscr{P}_{1m}$ can be neglected to the first order in the fluctuations. (The CMB dipole in the baryon rest frame is first-order in perturbation theory, and thus in principle should be considered – however it has the wrong parity to contribute to $\mathscr{P}_{1m}$.)

When we sum up the contributions of absorption and emission from Eqs. (32), (34) and (37), we get the net rate of change of the atom density matrix due to radiative processes. Using explicit expressions for the irreducible components $\mathcal{F}_{jm}$ of the phase-space density matrix from Eq. (B10), we find that

$$\dot{\mathscr{P}}_{00}|_\gamma = -A \left[\mathscr{P}_{00} - (3 - 4\mathscr{P}_{00}) \overline{f_{\rm I,00}} \right] \quad \text{and} \tag{38a}$$
$$\dot{\mathscr{P}}_{2m}|_\gamma = -A \Big[\left(1 + \overline{f_{\rm I,00}}\right) \mathscr{P}_{2m} - \frac{3 - 4\mathscr{P}_{00}}{5\sqrt{2}}$$
$$\times \left(\overline{f_{\rm I,2m}} + \sqrt{6}\,\overline{f_{\rm E,2m}} \right) \Big]. \tag{38b}$$

VI. OTHER PROCESSES AFFECTING THE ATOMIC DENSITY MATRIX

The level populations or spin-polarization of the hydrogen ground state can be altered by mechanisms other

than emission/absorption of the 21-cm photons. The ones relevant to the subject of this paper are background magnetic fields, hydrogen-hydrogen collisions, optical pumping by Lyman-α photons. Of these, the effect of the magnetic fields is simplest to evaluate.

The transition rates for the isotropically occupied cases due to the other processes have been calculated previously [66, 67]. In this section, we generalize these results to the case of spin-polarized hydrogen atoms – in particular we calculate the rates of de-polarization due to collisions and optical pumping, which are important for determining the lifetime of the excited state of Section III.

A. Background magnetic field

We choose the coordinate system such that the z-axis is oriented along the external magnetic field; in this case, the $F = 1$ states are split and the effect of the external field is to contribute a correction $\Delta E = g_e \mu_B B m_F / 2$ to the energy of each state. The elements of the density matrix then vary as $\dot{\rho}_{m_1 m_2} = i(g_e \mu_B B / 2\hbar)(m_2 - m_1)\rho_{m_1 m_2}$, and the irreducible components $\mathscr{P}_{jm}$ vary according to

$$\dot{\mathscr{P}}_{jm}|_B = i\frac{m}{2}\frac{g_e \mu_B}{\hbar}B\mathscr{P}_{jm}, \qquad (39)$$

where B is the local value of the magnetic field.

B. Spin-exchange collisions

The spin-polarization of primordial atomic gas can be modified by either spin-exchange collisions or by magnetic interactions [67, 68]. The former dominates under primordial conditions [67] so we focus on this process here. The rate coefficients and the resulting evolution of level populations have been calculated by Ref. [67] for a range of temperatures. In order to translate their results into evolution equations for the density matrix, we choose a basis where the density matrix is diagonal. This works because different irreducible moments $\mathscr{P}_{jm}$ of the atomic density matrix do not mix due to collisions in linear theory. Schematically,

$$\dot{\mathscr{P}}_{jm}|_c \sim C_j \mathscr{P}_{jm}. \qquad (40)$$

The collision coefficients C_j depend only on the rank of the polarization moment j, and not on its projection m. Therefore, we can compute the C_j by considering only cases where the $\mathscr{P}_{jm}$ with $m = 0$ are non-zero, i.e. where $\rho_{m_1 m_2}$ is diagonal [this follows from Eq. (15) and the $3 - j$ symbol selection rule $m = m_2 - m_1$]. The equations for the scalar components are slightly more complicated because there are two rank-zero objects that come into play, the occupancies of the singlet and the triplet.[6]

---

[6] Alternatively, the collisional evolution of a general density matrix has been studied earlier in Ref. [69].

In such a coordinate system, the rate equations in Ref. [67] take the form:

$$\dot{\rho}_{aa}|_c = - 3k_x^+ n_H \rho_{aa}^2 + 2(k^- + k^+) n_H \rho_{bb}\rho_{dd}$$
$$+ 2k^- n_H(\rho_{bb} + \rho_{dd})\rho_{cc} + k^+ n_H \rho_{cc}^2$$
$$- 2k_x^- n_H \rho_{aa}(\rho_{bb} + \rho_{cc} + \rho_{dd}), \qquad (41a)$$

$$\dot{\rho}_{bb}|_c = \dot{\rho}_{dd}|_c = k_x^+ n_H \rho_{aa}^2 + 2k_x^- n_H \rho_{aa}\rho_{cc} + k^0 n_H \rho_{cc}^2$$
$$- (k^0 + k^+ + 2k^-)n_H \rho_{bb}\rho_{dd}, \text{ and} \qquad (41b)$$

$$\dot{\rho}_{cc}|_c = k_x^+ n_H \rho_{aa}^2 + 2k_x^- n_H \rho_{aa}(\rho_{bb} - \rho_{cc} + \rho_{dd})$$
$$- 2k^- n_H(\rho_{bb} + \rho_{dd})\rho_{cc} - (k^+ + 2k^0)n_H \rho_{cc}^2$$
$$+ 2(k^- + k^0)n_H \rho_{bb}\rho_{dd}, \qquad (41c)$$

where $k^\pm$ and $k_x^\pm$ represent the thermal-average (de-)excitation rates computed in Ref. [67]. We write the evolution equations in (41) in terms of the irreducible moments $\mathscr{P}_{jm}$ following the argument leading to Eq. (40) and the explicit forms of Eq. (15). The resulting equations simplify greatly when we assume that the degree of spin-polarization is small, i.e. $\rho_{II} = \rho_{II}^{th} + \epsilon_I$ with the thermal populations of the sublevels $\rho_{bb}^{th} = \rho_{cc}^{th} = \rho_{dd}^{th} = \mathscr{P}_{00}^{th}/3, \rho_{aa}^{th} = 1 - \mathscr{P}_{00}^{th}$.

$$\dot{\rho}_{aa}|_c = -n_H \kappa(0\text{-}1)\rho_{aa} + n_H \kappa(1\text{-}0)\mathscr{P}_{00}, \qquad (42)$$

$$\dot{\mathscr{P}}_{00}|_c = n_H \kappa(0\text{-}1)\rho_{aa} - n_H \kappa(1\text{-}0)\mathscr{P}_{00}$$
$$= n_H \kappa(0\text{-}1) - n_H \left[\kappa(0\text{-}1) + \kappa(1\text{-}0)\right]\mathscr{P}_{00}, \qquad (43)$$

$$\dot{\mathscr{P}}_{1m}|_c = -n_H \kappa^{(1)}(1\text{-}0)\mathscr{P}_{1m}, \text{ and} \qquad (44)$$

$$\dot{\mathscr{P}}_{2m}|_c = -n_H \kappa^{(2)}(1\text{-}0)\mathscr{P}_{2m}, \qquad (45)$$

where the coefficients are extensions of the notation of Ref. [67] to include both transition and de-polarization rates. Under the simplifying assumptions stated above, these rates are:

$$\kappa(0\text{-}1) = 6k_x^+ (1 - \mathscr{P}_{00}^{th}) + 2k_x^- \mathscr{P}_{00}^{th}, \qquad (46a)$$

$$\kappa(1\text{-}0) = -2k_x^- (1 - \mathscr{P}_{00}^{th}) + \left(4k^- + 2k^+\right)\frac{\mathscr{P}_{00}^{th}}{3}, \qquad (46b)$$

$$\kappa^{(1)}(1\text{-}0) = 0, \text{ and} \qquad (46c)$$

$$\kappa^{(2)}(1\text{-}0) = 4k_x^- (1 - \mathscr{P}_{00}^{th}) + \frac{2}{3}\left(3k^0 + 2k^- + k^+\right)\mathscr{P}_{00}^{th}. \qquad (46d)$$

The de-polarization rate $\kappa^{(1)}(1\text{-}0)$ vanishes because the total spin angular momentum of the ensemble, corresponding to the orientation vector $\mathscr{P}_{1m}$, is conserved in collisions.

If the spin temperature is much larger than $T_* = 68$ mK, the states are nearly equally occupied and $\mathscr{P}_{00}^{th} \approx \frac{3}{4}$ [see Eq. (18)]. We use this in the rates of Eq. (46), along with the expressions for $k_x^\pm$ in terms of $k^\pm$ [67], and write down the collisional contributions to the evolution of the relevant pieces of the atom density matrix:

$$\dot{\mathscr{P}}_{00}|_c = -4n_H \kappa(1\text{-}0)\left(\mathscr{P}_{00} - \frac{3}{4} + \frac{3T_*}{16T_k}\right) \text{ and} \qquad (47a)$$
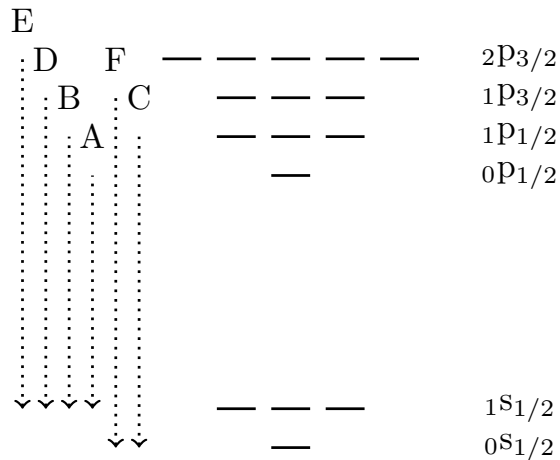
FIG. 4. The hyperfine structure of the ground and first excited electronic levels of the hydrogen atom. The levels are labeled by term symbols $_Fl_J$, where l is the spectroscopic notation for the orbital angular momentum, and J and F are the net electronic and total angular momentum respectively. Also shown are all the allowed single photon transitions between the 1s and 2p levels, along with their labels; these involve photons in the Lyα frequency range. Only the downward transitions are shown. The gaps between the levels are not drawn to scale.

$$\dot{\mathscr{P}}_{2m}|_c = -n_H\kappa^{(2)}(1\text{-}0)\mathscr{P}_{2m}, \qquad (47b)$$

with

$$\kappa^{(2)}(1\text{-}0) = 4\kappa(1\text{-}0) = 2(k^+ + k^-). \qquad (48)$$

These equations assume that the kinetic temperature $T_k \gg T_*$, which is valid over the entire range of redshifts.

C. Optical pumping by Lyman-α photons

Optical pumping by Lyman-α (Lyα) photons, or the Wouthuysen-Field effect, is another process that significantly affects the level populations within the hydrogen ground state (see e.g. Ref. [70]). An atom in the ground (1s) state absorbs a Lyα photon and gets excited to the 2p state. Subsequently, the atom re-emits a photon and returns to the ground state. However it does not necessarily de-excite to the same ground-state level it originated from. Thus, interactions with Lyα photons can change the density matrix of hydrogen atoms within the ground state basis.

The excited state consists of four levels: $_0p_{1/2}$, $_1p_{1/2}$, $_1p_{3/2}$ and $_2p_{3/2}$, where we use the notation $_Fl_J$ for the state in terms of its quantum numbers (see Fig. 4). We use Greek indices represent the excited levels i.e., those within 2p, when used as state labels.

The evolution of the ground state density matrix due to these transitions is governed by second-order pertur-

bation theory, and includes both contributions due to de-population of 1s (Lyα absorption) and re-population (the subsequent emission). The interaction Hamiltonian between the atom and radiation is

$$H_{\text{Ly}\alpha}^{\text{int}}(t) = \sum_{I,\mu,\alpha,\boldsymbol{k}_\gamma} Q_{\mu I}(\boldsymbol{k}_\gamma,\alpha)|\mu\rangle\langle I|a_\alpha(\boldsymbol{k}_\gamma) + \text{h.c.}, \quad (49)$$

where the matrix element $Q_{\mu I}(\boldsymbol{k}_\gamma,\alpha)$ is given by

$$Q_{\mu I}(\boldsymbol{k}_\gamma,\alpha) = -i\sqrt{2\pi\hbar\omega}\langle\mu|\boldsymbol{d}\cdot\boldsymbol{e}_\alpha(\hat{\boldsymbol{k}}_\gamma)|I\rangle . \qquad (50)$$

Here $\boldsymbol{d}$ is the electric dipole moment of the atom, which is proportional to the position vector $\boldsymbol{r}$ of the electron. The frequency corresponding to the energy difference between the upper (μ) and lower (I) state is $\omega_{\mu I} = (E_\mu - E_I)/\hbar$. The re-population equation is a straightforward extension of Fermi's Golden rule to second order; we have followed the derivation of Eq. (III,11) of Ref. [71], but with (i) our normalization conventions; (ii) without performing the integration over the outgoing photon wave-vector; and (iii) without averaging over initial photon frequencies.[7] This yields:

$$
\begin{aligned}
\dot{\rho}_{IJ}|_{\text{repop}} &= \hbar^{-4} \sum_{\boldsymbol{k}_\gamma,\boldsymbol{k}'_\gamma,\alpha,\beta,\mu,K,\nu,L} f(\boldsymbol{k}_\gamma)\, Q_{\mu I}^*(\boldsymbol{k}'_\gamma,\beta)Q_{\mu K}(\boldsymbol{k}_\gamma,\alpha) \\
&\times \frac{Q_{\nu J}(\boldsymbol{k}'_\gamma,\beta)Q_{\nu L}^*(\boldsymbol{k}_\gamma,\alpha)\,\pi\delta(\omega'-\omega+\omega_{JL})}{[i(\omega-\omega_{\mu K})-\Gamma_{2p}/2][-i(\omega-\omega_{\nu L})-\Gamma_{2p}/2]}\rho_{KL} \\
&+ \text{c.c.}
\end{aligned}
\qquad (51)
$$

The symbol $\boldsymbol{k}_\gamma$ is the absorbed photon's wave-vector, ω its frequency, α its polarization index ($\boldsymbol{k}'_\gamma$, ω', and β are used for the re-emitted photon). The phase-space density of photons is denoted by $f(\boldsymbol{k}_\gamma)$, and Γ_{2p} is the Einstein A-coefficient of the Lyα transition.

We can use Eq. (51) to infer a cross-section for the KL^{th} component of the density matrix ρ to transition into the IJ^{th} component. We simplify Eq. (51) by using Eq. (50) for the dipole matrix elements, and approximating the incident Lyα radiation field to be isotropic for performing integrals over the directions $\hat{\boldsymbol{k}}_\gamma$ and $\hat{\boldsymbol{k}}'_\gamma$. This is an excellent approximation due to the large value of the cross-section, and low mean free path for incident Lyα photons. Thus we conclude that Eq. (51) connects only irreducible components of the same rank within the initial and final density matrix.

---

[7] We have introduced the latter two modifications because we have multiple excited levels that can interfere with each other, since the hyperfine splitting and natural broadening of the 2p levels are of the same order of magnitude. Note that Eq. (51) could be viewed diagrammatically as the amplitude for the transition $|L\rangle \to |\nu\rangle \to |J\rangle$ (including a "propagator" for state $|\nu\rangle$), multiplied by the complex conjugate of that for $|K\rangle \to |\mu\rangle \to |I\rangle$ since we are following a density matrix rather than an amplitude.

Let the initial and final states, (I and J), belong to multiplets with total angular momentum quantum numbers F_I and F_J respectively. We implement the above program to infer the cross-section for a general irreducible component of rank-j within the initial state sub-matrix to go to the corresponding component within the final state sub-matrix. We use the suggestive notation $\sigma_{F_I \to F_J, (j)}$ to represent this cross-section; for example, the contribution to the density matrix from $F = 1 \to 1$ scattering is

$$\dot{\mathscr{P}}_{jm}|_{\text{repop}, F=1 \to 1} = 4\pi \int d\nu \, J_{\text{Ly}\alpha}(\nu) \sigma_{1 \to 1, (j)}(\nu) \mathscr{P}_{jm}. \tag{52}$$

The expression for $\sigma_{F_I \to F_J, (j)}$ can be read off from Eq. (51). We approximate all multiplicative factors of frequencies by the value of the Lyα line-center, and get (using e.g. the methodology of Ref. [66])

$$\sigma_{F_I \to F_J, (j)}(\omega)$$
$$= \frac{8\pi}{9} \frac{\omega_{\text{Ly}\alpha}^4}{c^4} \frac{e^4}{\hbar^2} \sqrt{2j+1} \sqrt{\frac{2F_J+1}{2F_I+1}} \sum_{m_{J_1}, m_{J_2}} \sum_{m_{I_1}, m_{I_2}}$$
$$\sum_{j', m'} \sum_{p,q} \sum_{r,s} \sum_{\mu,\nu} (-1)^{F_J - m_{J_2}} \begin{pmatrix} F_J & j & F_J \\ -m_{J_2} & m & m_{J_1} \end{pmatrix}$$
$$\times (-1)^{F_I - m_{I_2}} \begin{pmatrix} F_I & j' & F_I \\ -m_{I_2} & m' & m_{I_1} \end{pmatrix} g_{pr} g_{qs}$$
$$\times \frac{\langle F_J m_{J_1} | r^p | \mu \rangle \langle \mu | r^q | F_I m_{I_1} \rangle}{\Delta\omega_{\mu I} + i\Gamma_\mu/2}$$
$$\times \frac{\langle F_I m_{I_2} | r^s | \nu \rangle \langle \nu | r^r | F_J m_{J_2} \rangle}{\Delta\omega_{\nu I} - i\Gamma_\nu/2}, \tag{53}$$

where $\Delta\omega_{\mu I} = \omega - \omega_{\mu I}$ is the frequency offset from the line-center of the $\mu \to I$ transition, and $g_{pr} = (-1)^p \delta_{p, -r}$ is the metric tensor. The two 3-j symbols project the irreducible components of rank j and j' (which equals j) in the initial and final density sub-matrices in Eq. (51). We further simplify this result using the Wigner-Eckart theorem, and collapse the sum of six 3-j symbols:

$$\sigma_{F_I \to F_J, (j)}(\omega) = \frac{8\pi}{9} \frac{\omega_{\text{Ly}\alpha}^4}{c^4} \frac{e^4}{\hbar^2} \sqrt{\frac{2F_J+1}{2F_I+1}} \sum_{\mu,\nu} (-1)^{F_I - F_J}$$
$$\times \frac{\langle \mu \| r \| J \rangle^* \langle \mu \| r \| I \rangle \langle \nu \| r \| I \rangle^* \langle \nu \| r \| J \rangle}{(\Delta\omega_{\mu I} + i\Gamma_\mu/2)(\Delta\omega_{\nu I} - i\Gamma_\nu/2)}$$
$$\times \begin{Bmatrix} F_\mu & F_\nu & j \\ F_I & F_I & 1 \end{Bmatrix} \begin{Bmatrix} F_\mu & F_\nu & j \\ F_J & F_J & 1 \end{Bmatrix}. \tag{54}$$

When we perform the summation over the upper levels (μ and ν), the terms with $\mu = \nu$ and $\mu \neq \nu$ give Lorentzian line and interference profiles respectively. In this calculation, we assumed that the only factor involved in broadening the lines shown in Fig. 4 is their finite lifetime; in reality, the lines are broadened due to a combination of this and the Doppler effect, owing to which we need to convolve these profiles with the appropriate velocity distributions.

In the case where the triplet sublevels are equally occupied, the only relevant components of the density sub-matrices are those of rank zero. For $j = 0$, Eq. (54) gives net transition cross-sections from $F = 1 \to F = 0$ and $F = 0 \to F = 1$, which have been previously worked out. We use the notation and list of line strengths in Appendix B of Ref. [66]. In particular, Fig. 4 shows their choice of labels for the various lines making up the fine-structure of the Lyα line, which we will use in subsequent expressions.

Using the line-strengths in Ref. [66] for the irreducible matrix elements in Eq. (54), the isotropic cross-sections $\sigma_{F_I \to F_J, (0)}$ are given by Eqs. (B17,B18) of Ref. [66]. The one new cross section we need is the rank-2 cross section,

$$\sigma_{1 \to 1, (2)} = \frac{3}{2} \lambda_{\text{Ly}\alpha}^2 \gamma_{2p} \left(\frac{1}{27} \phi_{\text{BB}} + \frac{1}{108} \phi_{\text{DD}} + \frac{7}{36} \phi_{\text{EE}} \right.$$
$$\left. + \frac{2}{9} \phi_{\text{AE}} + \frac{1}{27} \phi_{\text{BD}} + \frac{1}{3} \phi_{\text{BE}} + \frac{1}{6} \phi_{\text{DE}} \right), \tag{55}$$

where $\gamma_{2p} = \Gamma_{2p}/4\pi = 50$ MHz and ϕ_{AB} etc. are the Lorentzian profiles defined by Eq. (B16) of Ref. [66].

We also need the depopulation rates (or equivalent cross-section). These rates are independent of the rank of the irreducible component (or the magnetic quantum numbers) because of the isotropy of the Lyman-α radiation – all of the 1s $F = 1$ states are de-populated at the same rate. Since the net population of the 2p levels is always negligible, the rate of depopulation from a level is given by the sum of the rates of all repopulations which start from that level:

$$\sigma_{F_I}|_{\text{depop}} = \sum_{F_J} \sigma_{F_I \to F_J, (0)}. \tag{56}$$

We obtain the following evolution equations for the irreducible components of interest by subtracting the contribution of depopulation from that of repopulation:

$$\dot{\mathscr{P}}_{00}|_{\text{Ly}\alpha} = -4\pi \int d\nu J_{\text{Ly}\alpha}(\nu) \left[\sigma_{1 \to 0, (0)}(\nu) \mathscr{P}_{00} \right.$$
$$\left. - \sigma_{0 \to 1, (0)}(\nu) \rho_{aa} \right], \tag{57}$$

$$\dot{\mathscr{P}}_{2m}|_{\text{Ly}\alpha} = -4\pi \int d\nu J_{\text{Ly}\alpha}(\nu) \left[\sigma_{1 \to 1, (0)}(\nu) + \sigma_{1 \to 0, (0)}(\nu) \right.$$
$$\left. - \sigma_{1 \to 1, (2)}(\nu) \right] \mathscr{P}_{2m}. \tag{58}$$

To simplify these equations, we use the relation $\rho_{aa} = 1 - \mathscr{P}_{00}$, and substitute the repopulation cross-sections.

The effect of optical pumping by Lyα photons on the rank zero component (net triplet occupancy) is complicated by a source term. In the approximation of a very high cross-section (or $T > \infty$), the states are driven to equal occupancy i.e. $\mathscr{P}_{00} \to 3/4$. In order to correct the populations for a finite temperature, we need to consider the frequency dependence of the flux $J_{\text{Ly}\alpha}$. This motivates the definition of the flux correction factor $\tilde{S}_\alpha$ [8] and

—————

[8] The tilde is to avoid conflict with the usual definition of S_α in the

the effective color temperature $T_{c,\text{eff}}$, which are given by

$$T_{c,\text{eff}} = -\frac{h}{k_B}\frac{d}{d\nu}\ln J_{\text{Ly}\alpha}(\nu) \tag{59}$$

and

$$\tilde{S}_\alpha = \frac{9}{8\lambda_{\text{Ly}\alpha}^2\gamma_{2p}}\int d\nu \frac{J_{\text{Ly}\alpha}(\nu)}{J_\alpha}[\sigma_{1\to0,(0)}(\nu) + \sigma_{0\to1,(0)}(\nu)], \tag{60}$$

where J_α is the flux on the blue side of the Lyman-α line, before it is processed by any radiative transfer. Substitution of these definitions in Eq. (57) gives us the evolution equation for the occupancy:

$$\dot{\mathscr{P}}_{00}|_{\text{Ly}\alpha} = -\frac{32}{9}\pi\lambda_{\text{Ly}\alpha}^2\gamma_{2p}\tilde{S}_\alpha J_\alpha\left[\mathscr{P}_{00} - \frac{3}{4} + \frac{3T_*}{16T_{c,\text{eff}}}\right]. \tag{61}$$

The evolution of the rank two irreducible component of the triplet state density sub-matrix is easier to evaluate, since it has no source term. The detailed frequency dependence of the flux $J_{\text{Ly}\alpha}$ is not crucial. Substituting the expressions for the cross-sections, we obtain the following depolarization rate:

$$\dot{\mathscr{P}}_{2m}|_{\text{Ly}\alpha} = -0.601 \times 6\pi\lambda_{\text{Ly}\alpha}^2\gamma_{2p}\tilde{S}_{\alpha,(2)}J_\alpha\mathscr{P}_{2m}, \tag{62}$$

where the flux correction factor $\tilde{S}_{\alpha,(2)}$ for the rank-two tensor is defined such that

$$0.601\tilde{S}_{\alpha,(2)}J_\alpha = \int d\nu J_{\text{Ly}\alpha}(\nu)\left(\frac{1}{9}\phi_{AA} + \frac{5}{27}\phi_{BB} + \frac{11}{108}\phi_{DD}\right.$$
$$\left. + \frac{13}{36}\phi_{EE} - \frac{2}{9}\phi_{AE} - \frac{1}{27}\phi_{BD} - \frac{1}{3}\phi_{BE} - \frac{1}{6}\phi_{DE}\right), \tag{63}$$

and the numerical pre-factor is the integral over frequency of the term enclosed in braces on the RHS of the above equation.

VII. RADIATIVE TRANSFER

Sections V and VI dealt with the evolution of the atom's density matrix due to various processes. In this section, we study the evolution of the components of the 21-cm radiation's phase-space density matrix $f_{X,jm}(\omega)$. In particular, the intensity monopole $f_{I,00}$ and quadupole $f_{I,2m}$ are the relevant multipoles to study for the effect on the brightness temperature.

The baryon rest frame simplifies the details of the matter-radiation interaction, hence we use it throughout this calculation. We restrict ourselves to quantities

---

literature, which approximates the color temperature, $T_{c,\text{eff}}$ with the kinetic temperature, T_k. It is consistent with the notation of Ref. [66].

which are atmost of the first order in smallness in terms of the matter overdensity δ.

The only quantity related to the radiation field with a zeroth-order piece is the intensity monopole $f_{I,00}$. From the discussion in Section I, we expect the matter velocity $\boldsymbol{v}$ and the intensity and polarization quadrupoles, $f_{I,2m}$ and $f_{E,2m}$, to be quantities of the first order in smallness.

The Boltzmann equation for a generic component of the phase space density f_X is

$$\frac{Df_X}{Dt} = \dot{f}_X|_s. \tag{64}$$

The left hand side is the material derivative with respect to the flow of points in phase space, which represents the effect of free-streaming. The right hand side is the source term for the phase-space density, due to interaction with atoms.

A. Free-streaming term

The material derivative of the phase-space density expands to

$$\frac{Df}{Dt} = \dot{f} + \frac{d\boldsymbol{x}}{dt}\cdot\boldsymbol{\nabla}f + \frac{d\omega}{dt}\frac{\partial f}{\partial\omega} + \frac{d\hat{\boldsymbol{n}}}{dt}\cdot\nabla_{\hat{n}}f, \tag{65}$$

where, as earlier, $\hat{\boldsymbol{n}}$ is the radiation's direction of propagation. The second, third, and fourth terms represent advection, time-dependent redshift, and lensing respectively. Since we are interested only in terms up to the first order in the density fluctuations, we neglect lensing (since it is a second-order effect), and replace the coefficient of $\boldsymbol{\nabla}f$ in the advection term with its zeroth-order value, which is

$$\frac{d\boldsymbol{x}}{dt} = c\,\hat{\boldsymbol{n}}. \tag{66}$$

In order to expand the redshift term, we use the relation between the angular frequency of a photon in the baryon rest frame (ω) and in the Newtonian frame (ω_N):

$$\omega = \omega_N\left(1 - \frac{\boldsymbol{v}\cdot\hat{\boldsymbol{n}}}{c}\right), \tag{67}$$

where $\boldsymbol{v}$ and $\hat{\boldsymbol{n}}$ are the bulk matter velocity and the direction of the photon's travel respectively. The coefficient of the time-dependent redshift term is

$$\frac{1}{\omega}\frac{d\omega}{dt} = \frac{1}{\omega_N}\frac{d\omega_N}{dt} - \frac{1}{c}\frac{d}{dt}(\boldsymbol{v}\cdot\hat{\boldsymbol{n}}) + \dots$$
$$= \frac{1}{\omega_N}\frac{d\omega_N}{dt} - \frac{1}{c}\dot{v}_i n_i - \frac{\partial v_i}{\partial x_j}n_i n_j + \dots \tag{68}$$

The first term, which is the rate of redshifting in the Newtonian frame, has contributions both from large-scale Hubble flow and gravitational redshifting in the presence of local potential wells [72]. The latter contribution is

the Sachs-Wolfe effect. The second term is the time-dependent redshift due to local acceleration, and is of the same size as the Sachs-Wolfe term. The final term, which is the origin of the effect of interest, is the contribution of the local matter velocity gradient $\boldsymbol{\nabla} \boldsymbol{v}$.

The effect of local velocity gradients is much larger than that of acceleration, which scales as the depth of the potential wells, as long as the modes under consideration are sub-horizon sized. We estimate their relative sizes as

$$\frac{(1/c)\dot{v}_i n_i}{(\partial v_i/\partial x_j)n_i n_j} \approx \frac{aH}{kc} \approx 4 \times 10^{-4}$$
$$\times \left(\frac{1+z}{10}\right)^{1/2}\left(\frac{k}{1\ \mathrm{Mpc}^{-1}}\right)^{-1}\left(\frac{\Omega_m h^2}{0.143}\right)^{1/2}. \quad (69)$$

The second term in Eq. (65) is the advection term. On free streaming, it causes mixing of multipoles on a characteristic timescale $\sim (a/kc)$ [62]. The size of this contribution relative to the time-dependent redshift term is set by the comparision with the timescale for the photons to redshift through the line. We can safely neglect the advection term as long as we restrict ourselves to modes of wavelengths much larger than the Jeans length, r_{J}, at this epoch. This is a good approximation for the modes under consideration:

$$\frac{c(\partial f/\partial x_i)n_i}{H\omega(\partial f/\partial \omega)} \sim \frac{k}{a}\frac{v_{\mathrm{s}}}{H} \sim \frac{kr_{\mathrm{J}}}{a} \approx 5.8 \times 10^{-3}$$
$$\times \left(\frac{T_{\mathrm{k}}}{T_\gamma}\right)^{1/2}\left(\frac{k}{1\ \mathrm{Mpc}^{-1}}\right)\left(\frac{\Omega_{\mathrm{m}} h^2}{0.143}\right)^{-1/2}. \quad (70)$$

Hence the most important contribution to the time-dependent redshift term is the velocity gradient term. We assume that the fluctuation is a plane wave with co-moving wave-vector $\boldsymbol{k}$, and use the continuity equation to express the velocity gradient in terms of the overdensity as follows:

$$\frac{1}{\omega}\frac{\mathrm{d}\omega}{\mathrm{d}t} \approx -H - \frac{\partial v_i}{\partial x_j}n_i n_j = -H\left[1 - \delta(\hat{\boldsymbol{k}}\cdot\hat{\boldsymbol{n}})^2\right], \quad (71)$$

where H is the Hubble rate at the redshift under consideration and δ is the local overdensity. In writing this equation, we used the standard scaling of the growth factor for a matter dominated universe, i.e. $d(\log\delta)/d(\log a) = 1$.

Thus the free-streaming term of Eq. (65) is

$$\frac{\mathrm{D}f}{\mathrm{D}t} = \dot{f} - H\left[1 - \delta(\hat{\boldsymbol{k}}\cdot\hat{\boldsymbol{n}})^2\right]\omega\frac{\partial f}{\partial\omega}. \quad (72)$$

In a coordinate system with an arbitrary orientation,

$$(\hat{\boldsymbol{k}}\cdot\hat{\boldsymbol{n}})^2 = \frac{8\pi}{15}\sum_m Y_{2m}(\hat{\boldsymbol{k}})\left[Y_{2m}(\hat{\boldsymbol{n}})\right]^* + \frac{1}{3}. \quad (73)$$

Using this identity, we write down the free-streaming terms for the relevant moments in a general coordinate system.

In order to expand Eq. (72) into moments, we note that the only relevant moments i.e. those which are non-zero up to first order in the matter density fluctuation δ, are the intensity monopole $f_{\mathrm{I},00}$ (which has a zeroth-order piece too) and quadrupole $f_{\mathrm{I},2m}$, and the polarization quadrupole $f_{\mathrm{E},2m}$ (vide Section III and Table III). Thus, up to first order in δ, the equations describing the free-streaming of the relevant moments are

$$\frac{\mathrm{D}f_{\mathrm{I},00}}{\mathrm{D}t} = \dot{f}_{\mathrm{I},00} - H\left[1 - \frac{\delta}{3}\right]\omega\frac{\partial f_{\mathrm{I},00}}{\partial\omega}, \quad (74a)$$

$$\frac{\mathrm{D}f_{\mathrm{I},2m}}{\mathrm{D}t} = \dot{f}_{\mathrm{I},2m} - H\omega\frac{\partial f_{\mathrm{I},2m}}{\partial\omega}$$
$$+ \frac{2}{3}\sqrt{\frac{4\pi}{5}}\delta H\omega\frac{\partial f_{\mathrm{I},00}}{\partial\omega}Y_{2m}(\hat{\boldsymbol{k}}), \text{ and} \quad (74b)$$

$$\frac{\mathrm{D}f_{\mathrm{E},2m}}{\mathrm{D}t} = \dot{f}_{\mathrm{E},2m} - H\omega\frac{\partial f_{\mathrm{E},2m}}{\partial\omega}. \quad (74c)$$

B. Source term

The source term describes the evolution of the 21-cm radiation's phase-space density matrix due to interaction with neutral hydrogen atoms. In this section, we generalize the usual treatment of spontaneous and stimulated emission, and photo-absorption to the case of spin-polarized atoms.

We complete construction of the plane wave source term $\dot{f}_{\alpha\beta}(\hat{\boldsymbol{n}},\omega)|_{\mathrm{s}}$ in several steps. First, we find the contribution to the plane wave source term from a single atom in terms of spherical operators. Then we sum this contribution over all atoms, with the specified number density $n_{\mathrm{H}}x_{1\mathrm{s}}$. Finally, we turn the required expectation values of spherical operators into photon phase space densities, and re-express them in terms of the radiation multipoles and atomic polarizations.

We write the second-order moments of the photon field in the plane wave basis in terms of the spherical basis by inversion of Eq. (B2):

$$a_\alpha(\boldsymbol{k}_\gamma) = \frac{(2\pi c)^{3/2}}{\omega}e^{-i\boldsymbol{k}_\gamma\cdot\boldsymbol{R}}\sum_{jm\lambda}\left[\boldsymbol{e}^*_{(\alpha)}\cdot\boldsymbol{Y}^{(\lambda)}_{jm}\right](\hat{\boldsymbol{k}}_\gamma)\,a^{(\lambda)}_{jm}(\omega), \quad (75)$$

where $\omega = k_\gamma/c$ and $\lambda \in \{\mathrm{E,M}\}$. We have inserted a factor of $e^{-i\boldsymbol{k}_\gamma\cdot\boldsymbol{R}}$ here to place the atom (which is the center around which we expand the spherical waves) at position $\boldsymbol{R}$ rather than the origin. It follows that the time evolution of the photon density matrix is

$$\frac{\mathrm{d}}{\mathrm{d}t}\langle a^\dagger_\alpha(\boldsymbol{k}_\gamma)a_\beta(\boldsymbol{k}'_\gamma)\rangle$$
$$= \frac{(2\pi c)^3}{\omega^2}\sum_{jm\lambda j'm'\lambda'}\left[\boldsymbol{e}_{(\alpha)}\cdot\boldsymbol{Y}^{(\lambda)*}_{jm}\right](\hat{\boldsymbol{k}}_\gamma)\left[\boldsymbol{e}^*_{(\beta)}\cdot\boldsymbol{Y}^{(\lambda')}_{j'm'}\right](\hat{\boldsymbol{k}}'_\gamma)$$
$$\times e^{i(\boldsymbol{k}_\gamma-\boldsymbol{k}'_\gamma)\cdot\boldsymbol{R}}\frac{\mathrm{d}}{\mathrm{d}t}\langle a^{(\lambda)\dagger}_{jm}(\omega)a^{(\lambda')}_{j'm'}(\omega')\rangle. \quad (76)$$

This result is valid if the electromagnetic field interacts with a single atom. However, in the scenario un-

der consideration, it interacts with an ensemble of atoms of number density $n_H x_{1s}$. We obtain such an ensemble by integrating Eq. (76) over volume $d^3 \boldsymbol{R}$ and multiplying by $n_H x_{1s}$. Using the rule that $\int e^{i(\boldsymbol{k}_\gamma - \boldsymbol{k}'_\gamma) \cdot \boldsymbol{R}} d^3 \boldsymbol{R} = (2\pi)^3 \delta^{(3)}(\boldsymbol{k}_\gamma - \boldsymbol{k}'_\gamma)$, we obtain a δ-function on the right hand side and hence the result:

$$\dot{f}_{\beta\alpha}(\omega, \hat{\boldsymbol{k}}_\gamma)|_s = \frac{(2\pi c)^3}{\omega^2} n_H x_{1s} \sum_{jm\lambda j'm'\lambda'} \left[\boldsymbol{e}_{(\alpha)} \cdot \boldsymbol{Y}_{jm}^{(\lambda)*}\right](\hat{\boldsymbol{k}}_\gamma)$$
$$\times \left[\boldsymbol{e}_{(\beta)}^* \cdot \boldsymbol{Y}_{j'm'}^{(\lambda')}\right](\hat{\boldsymbol{k}}_\gamma) \frac{d}{dt} \langle a_{jm}^{(\lambda)\dagger}(\omega) a_{j'm'}^{(\lambda')}(\omega) \rangle. \tag{77}$$

Note that in Eq. (77), the derivative on the right-hand side is the contribution of a single atom.

Since the operator $a_{jm}^{(\lambda)\dagger}(\omega) a_{j'm'}^{(\lambda')}(\omega)$ commutes with the radiation's Hamiltonian H_γ, it evolves only in accordance with the interaction Hamiltonian $H_{hf,\gamma}$, specifically:

$$\frac{d}{dt} \langle a_{jm}^{(\lambda)\dagger}(\omega) a_{j'm'}^{(\lambda')}(\omega) \rangle$$
$$= \frac{i}{\hbar} \left\langle \left[H_{hf,\gamma}, a_{jm}^{(\lambda)\dagger}(\omega) a_{j'm'}^{(\lambda')}(\omega)\right] \right\rangle$$
$$= \frac{i}{\hbar} \sum_{m_F} V_{m_F a,m}(\omega) \left\langle |1m_F\rangle\langle 00| a_{j'm'}^{(\lambda')}(\omega) \right\rangle \delta_{M\lambda} \delta_{j1}$$
$$+ \text{c.c.s.}$$
$$= -\frac{\pi}{\hbar^2} \sum_{m_F m_2 m_3} V_{m_F a,m}(\omega) V_{m_2 a,m_3}^*(\omega) \delta(\omega - \omega_{hf}) \delta_{M\lambda} \delta_{j1}$$
$$\times \left[\delta_{m_2 m_F} \rho_{aa} f_{m'm_3}^{(\lambda'j')(\text{M1})}(\omega) - \rho_{m_2 m_F}(\delta_{\lambda'M} \delta_{j'1} \delta_{m'm}\right.$$
$$\left. + f_{m'm_3}^{(\lambda'j')(\text{M1})}(\omega))\right] + \text{c.c.s.} \tag{78}$$

Here again "c.c.s." stands for complex conjugation with a swap (i.e. swap $\lambda jm \leftrightarrow \lambda'j'm'$). In the second equality we used Eq. (29) for $H_{hf,\gamma}$, and in the third we use the results of Appendix C for the atom-radiation three-point function.

We next use Eq. (28) for the interaction matrix elements, with which Eq. (78) simplifies to

$$\frac{d}{dt} \langle a_{jm}^{(\lambda)\dagger}(\omega) a_{j'm'}^{(\lambda')}(\omega) \rangle$$
$$= -\frac{A}{2} \delta(\omega - \omega_{hf}) \delta_{M\lambda} \delta_{j1} \sum_{m_2} \left\{\delta_{m_2 m} \rho_{aa} f_{m'm_2}^{(\lambda'j')(\text{M1})}(\omega)\right.$$
$$\left. - \rho_{m_2 m}[\delta_{\lambda'M} \delta_{j'1} \delta_{m'm_2} + f_{m'm_2}^{(\lambda'j')(\text{M1})}(\omega)]\right\} + \text{c.c.s.} \tag{79}$$

A useful definition is the isotropic absorption cross-section $\sigma(\omega)$ for radiation whose wavelength is close to 21-cm:

$$\sigma(\omega) = 3\pi^2 \frac{c^2}{\omega^2} A \phi(\omega), \tag{80}$$

where $\phi(\omega)$ is the absorption profile centered at ω_{hf}. It is broadened from the delta function of Eq. (79) due to the thermal motions of the hydrogen atoms.

Substituting Eq. (79) into Eq. (77), using the definition (80) and the notation $\hat{\boldsymbol{n}}$ for the direction of propagation, we get

$$\dot{f}_{\beta\alpha}(\omega, \hat{\boldsymbol{n}})|_s$$
$$= -\frac{4\pi}{3} n_H x_{1s} \sigma(\omega) c \sum_{m_2 m j'm'\lambda'} \left[\boldsymbol{e}_{(\alpha)} \cdot \boldsymbol{Y}_{1m}^{(M)*}\right](\hat{\boldsymbol{n}})$$
$$\times \left[\boldsymbol{e}_{(\beta)}^* \cdot \boldsymbol{Y}_{j'm'}^{(\lambda')}\right](\hat{\boldsymbol{n}}) \left\{\delta_{m_2 m} \rho_{aa} f_{m'm_2}^{(\lambda'j')(\text{M1})}(\omega)\right.$$
$$\left. - \rho_{m_2 m}[\delta_{\lambda'M} \delta_{j'1} \delta_{m'm_2} + f_{m'm_2}^{(\lambda'j')(\text{M1})}(\omega)]\right\}$$
$$+ [\alpha \leftrightarrow \beta]^*. \tag{81}$$

(note that because of the symmetry of Eq. 77 under $\lambda jm \leftrightarrow \lambda'j'm'$ symmetry, the "c.c.s." term simply results in the complex conjugate of the contribution with α and β switched, thereby guaranteeing the Hermiticity of the phase-space density matrix).

It is profitable to break Eq. (81) into the three terms in braces: these correspond to absorption, spontaneous emission, and stimulated emission, respectively. Each one may be converted back into radiation multipole moments using the inverse of Eq. (25):

$$(\dot{f}_{\beta\alpha})_{jm}(\omega)|_s = \sqrt{\frac{2j+1}{4\pi}} \int \dot{f}_{\beta\alpha}(\omega, \hat{\boldsymbol{n}})|_s [_{\beta-\alpha}Y_{jm}(\hat{\boldsymbol{n}})] d^2 \boldsymbol{n}. \tag{82}$$

This conversion entails the angular integral of products of three spherical harmonics, and results in appropriate sets of 3-j symbols [65].

The absorption term is

$$(\dot{f}_{\alpha\beta})_{jm}(\omega)|_{ab} = -n_H x_{1s} \sigma(\omega) c \, \rho_{aa} (f_{\alpha\beta})_{jm}(\omega). \tag{83}$$

The emission terms involve elements of the triplet state density sub-matrix ρ_{mn}, which are most naturally expressed in terms of the irreducible components $\mathscr{P}_{jm}$ using Eq. (15). The spontaneous emission term simplifies to

$$(\dot{f}_{\alpha\beta})_{jm}(\omega)|_{sp.em} = n_H x_{1s} \frac{\sigma(\omega)c}{3} \sqrt{3(2j+1)}$$
$$\times \alpha\beta \begin{pmatrix} 1 & 1 & j \\ \alpha & -\beta & \beta-\alpha \end{pmatrix} \mathscr{P}_{jm}, \tag{84}$$

and the stimulated emission term simplifies to

$$(\dot{f}_{\alpha\beta})_{jm}|_{st.em}$$
$$= \frac{2j+1}{2} n_H x_{1s} \frac{\sigma(\omega)c}{3} (-1)^m \sum_{j_1 m_1 j_2 m_2 \gamma}$$
$$\sqrt{3(2j_2+1)} \left[\alpha\gamma \begin{pmatrix} j_1 & j_2 & j \\ -m_1 & -m_2 & m \end{pmatrix} \begin{pmatrix} 1 & 1 & j_2 \\ \alpha & -\gamma & \gamma-\alpha \end{pmatrix}\right.$$
$$\times \begin{pmatrix} j_1 & j_2 & j \\ \gamma-\beta & \alpha-\gamma & \beta-\alpha \end{pmatrix} (f_{\gamma\beta})_{j_1 m_1} \mathscr{P}_{j_2 m_2}\right]$$
$$+ (-1)^{-m} [\alpha \leftrightarrow \beta, m \to -m]^*. \tag{85}$$

We can further rewrite the source terms of (83), (84) and (85) in terms of the parity invariants of Eq. (26).

TABLE III. Sizes of terms. They are classified as follows -
A: Terms included in the usual, lowest-order calculation.
B: Terms relevant to the effect under consideration.
C: Other terms of the same order.

Quantity	Sizes of relevant constituents		
	A	B	C
$f_{I,00}(\mathcal{X})$	$T_\gamma/T_* + ()\,\tau$		$()\,\tau^2$
$f_{I,2m}(\mathcal{X})$	$()\,\delta\tau$	$()\,\delta\tau^2$	
$f_{E,2m}(\mathcal{X})$			$()\,\delta\tau^2$
$\mathscr{P}_{2m}$		$()\,\delta\tau$	

As noted earlier in Section VII A, the only relevant moments are the intensity monopole $f_{I,00}$ and quadrupole $f_{I,2m}$, and the polarization quadrupole $f_{E,2m}$. Summing up all the contributions yields the following source terms for these moments:

$$\dot{f}_{I,00}(\omega)\big|_s = n_H x_{1s} \frac{\sigma(\omega)c}{3}\left[-(3-4\mathscr{P}_{00})f_{I,00} + \mathscr{P}_{00}\right],\tag{86a}$$

$$\dot{f}_{I,2m}(\omega)\big|_s = n_H x_{1s}\frac{\sigma(\omega)c}{3}\Big[-(3-4\mathscr{P}_{00})f_{I,2m} \\ + \frac{1}{\sqrt{2}}(1+f_{I,00})\mathscr{P}_{2m}\Big], \text{ and} \tag{86b}$$

$$\dot{f}_{E,2m}(\omega)\big|_s = n_H x_{1s}\frac{\sigma(\omega)c}{3}\Big[-(3-4\mathscr{P}_{00})f_{E,2m} \\ + \sqrt{3}(1+f_{I,00})\mathscr{P}_{2m}\Big].\tag{86c}$$

VIII. SOLUTION FOR THE BRIGHTNESS TEMPERATURE

In this section, we collect the results of the previous sections, and derive their effect on observables i.e. the 21-cm brightness temperature fluctuations.

Let us first consider the Boltzmann equation [Eq. (64)]. It is useful to define a few quantities to facilitate its solution and interpretation.

First, the optical depth τ of the neutral hydrogen gas is proportional to the absorption cross section integrated over the line. For a given Hubble rate H, and a peculiar velocity along the line of sight $v_{||}$,

$$\tau = \frac{\pi^2 c^3 n_H x_{1s} A (3-4\mathscr{P}_{00})}{H\omega_{hf}^3[1+(1/H)(dv_{||}/dr_{||})]}$$
$$= 9.7\times10^{-3}\times x_{1s}\left(\frac{T_\gamma}{T_s}\right)\left[1+\frac{4}{3}\delta\right]\left(\frac{\Omega_b h^2}{0.022}\right)$$
$$\times \left(\frac{\Omega_m h^2}{0.143}\right)^{-1/2}\left(\frac{1-Y_{He}}{0.75}\right)\left(\frac{1+z}{10}\right)^{1/2}.\tag{87}$$

This expression is correct to first order in the fluctuation δ, and assumes that the slow variation of factors of ω in front of the absorption profile in Eq. (80) can be neglected. Expression (87) is the optical depth for the monopole, since it is derived by averaging out the dependence of the velocity-gradient on direction.

Next is the cumulative function $\mathcal{X}(\omega)$ for the absorption profile $\phi(\omega)$, which is defined as

$$\mathcal{X}(\omega) = \int_{-\infty}^{\omega}d\omega'\,\phi(\omega').\tag{88}$$

It is convenient to express the frequency dependence of quantities in terms of $\mathcal{X}$, which varies between 0 and 1 from the red- to the blue-side of the line. The boundary conditions for the moments are fixed on the blue side of the line i.e. at $\mathcal{X} = 1$:

$$f_{I,00} = f_\gamma \approx \frac{T_\gamma}{T_*}\ \text{ and }\ f_{I,2m} = f_{E,2m} = 0\ \text{ at }\ \mathcal{X} = 1.\tag{89}$$

Finally, the 21-cm brightness temperature fluctuation relative to the CMB, δT_b, is defined via the phase-space density on the red side of the line:

$$\delta T_b(\hat{\boldsymbol{n}}) = \frac{T_*}{1+z}\left(f_I(\mathcal{X}=0,\hat{\boldsymbol{n}}) - f_\gamma\right)$$
$$\approx \frac{T_*}{1+z}\left(f_I(\mathcal{X}=0,\hat{\boldsymbol{n}}) - \frac{T_\gamma}{T_*}\right).\tag{90}$$

Before we write down the form of the Boltzmann equation, it is worthwhile to note the sizes of various relevant terms. Table III shows the sizes of the relevant pieces, and summarizes the estimates made in Section III.

We solve for the phase-space density in the steady state approximation. This holds if the time taken for the photon to redshift through the line is much smaller than a Hubble time, which is the case for a narrow line. Thus we safely neglect the time-derivatives in the free-streaming term [Eq. (74)], and take the source terms from Eq. (86). With the above definitions and assumptions, the Boltzmann equations for the various moments simplify to

$$\frac{\partial f_{I,00}}{\partial\mathcal{X}} = \tau\left[f_{I,00} - \frac{T_s}{T_*}\right],\tag{91a}$$

$$\frac{\partial f_{I,2m}}{\partial\mathcal{X}} = \tau\left[f_{I,2m} - \frac{2\sqrt{2}}{3}\frac{T_\gamma T_s}{T_*^2}\mathscr{P}_{2m}\right]$$
$$+ \frac{2}{3}\delta\frac{\partial f_{I,00}}{\partial\mathcal{X}}\sqrt{\frac{4\pi}{5}}Y_{2m}(\hat{\boldsymbol{k}}), \text{ and}\tag{91b}$$

$$\frac{\partial f_{E,2m}}{\partial\mathcal{X}} = \tau\left[f_{E,2m} - \frac{4\sqrt{3}}{3}\frac{T_\gamma T_s}{T_*^2}\mathscr{P}_{2m}\right].\tag{91c}$$

The velocity-gradient contribution to the optical depths of the quadrupoles is different, but these moments vanish in the absence of fluctuations. Hence Eq. (91) is correct to first order in the overdensity δ. The simplifications here use the sizes of various terms from Table III, the relation of Eq. (18) between the excited state occupancy $\mathscr{P}_{00}$ and the spin temperature T_s, and neglect spontaneous emission contributions.

The Boltzmann equation must be solved along with the evolution equations for the hydrogen atom-density

matrix. We obtain these from the Sections V and VI, and include the effects of interaction with radio photons, [Section V], optical pumping by Lyman-α photons [Section VI C], collisions with other hydrogen atoms [Section VI B] and precession within an external magnetic field [Section VI A]. Similar to the phase-space density, we solve for the various parts of the density matrix under the steady state approximation.

Firstly, we obtain the evolution of the excited state occupancy $\mathscr{P}_{00}$ (or alternatively, the spin temperature $T_{\rm s}$) by summing Eqs. (38a), (47a) and (61) and equating the result to zero:

$$
\begin{aligned}
\dot{\mathscr{P}}_{00} = &\, A\left[-\mathscr{P}_{00} + (3 - 4\mathscr{P}_{00})\,\overline{f_{\rm I,00}}\right] \\
&- \frac{32\pi\lambda_{\rm Ly\alpha}^2\gamma_{\rm 2p}}{9}\tilde{S}_\alpha J_\alpha \left(\mathscr{P}_{00} - \frac{3}{4} + \frac{3}{16}\frac{T_*}{T_{\rm c,eff}}\right) \\
&- 4\kappa(1\text{-}0)n_{\rm H}\left(\mathscr{P}_{00} - \frac{3}{4} + \frac{3}{16}\frac{T_*}{T_{\rm k}}\right) = 0. \quad (92)
\end{aligned}
$$

In a similar manner, we obtain the equation for the evolution of the alignment tensor $\mathscr{P}_{2m}$ by summing Eqs. (38b), (47b), (62) and (39). It is most convenient to continue in the coordinate system used in Section VI A, with the z−axis along the direction of the magnetic field; In this system, the angular indices jm are not mixed:

$$
\begin{aligned}
\dot{\mathscr{P}}_{2m} = &\, A\left[-\frac{T_\gamma}{T_*}\mathscr{P}_{2m} + \frac{3}{20\sqrt{2}}\frac{T_*}{T_{\rm s}}\overline{f_{\rm I,2m}}\right] \\
&- 3.607\pi\lambda_{\rm Ly\alpha}^2\gamma_{\rm 2p}\tilde{S}_{\alpha,(2)}J_\alpha\mathscr{P}_{2m} \\
&- n_{\rm H}\kappa^{(2)}(1\text{-}0)\mathscr{P}_{2m} + i\frac{m}{2}\frac{g_{\rm e}\mu_{\rm B}}{\hbar}B\mathscr{P}_{2m} \approx 0. \quad (93)
\end{aligned}
$$

As earlier, the above equation neglects spontaneous emission and is correct up to the sizes of terms from Table III. We carry out the averages over the line-profile in Eqs. (92) and (93) using

$$
\overline{f} = \int_{-\infty}^{\infty}{\rm d}\omega\, f(\omega) = \int_0^1{\rm d}\mathcal{X}\, f(\mathcal{X}). \quad (94)
$$

Equations (92) and (91a) together determine the spin temperature $T_{\rm s}$ and the intensity monopole $f_{\rm I,00}$, which is given in terms of the former by

$$
f_{\rm I,00}(\mathcal{X}) = \frac{1}{T_*}\left[T_{\rm s} + (T_\gamma - T_{\rm s})\,e^{-\tau(1-\mathcal{X})}\right]. \quad (95)
$$

Likewise, we use Eqs. (93) and (91b) to solve for the alignment tensor $\mathscr{P}_{2m}$, and the intensity quadrupole $f_{\rm I,2m}(\mathcal{X})$ in a simultaneous manner. They are given by the following solutions, which are correct to the orders in Table III:

$$
\begin{aligned}
\mathscr{P}_{2m} = &\, \frac{1}{20\sqrt{2}}\frac{T_*}{T_\gamma}\left(1 - \frac{T_\gamma}{T_{\rm s}}\right)\frac{\tau}{1 + x_{\alpha,(2)} + x_{\rm c,(2)} - imx_{\rm B}} \\
&\times \delta\sqrt{\frac{4\pi}{5}}Y_{2m}(\hat{\boldsymbol{k}})
\end{aligned} \quad (96)
$$

and

$$
\begin{aligned}
f_{\rm I,2m}(\mathcal{X}) = &\, \frac{T_{\rm s}}{T_*}\left(1 - \frac{T_\gamma}{T_{\rm s}}\right)\left[\frac{1}{30}\frac{\tau}{1 + x_{\alpha,(2)} + x_{\rm c,(2)} - imx_{\rm B}}\right. \\
&\left.+ \frac{2}{3}\left(1 - \tau(1 - \mathcal{X})\right)\right]\delta\tau(1 - \mathcal{X})\sqrt{\frac{4\pi}{5}}Y_{2m}(\hat{\boldsymbol{k}}),
\end{aligned} \quad (97)
$$

where the quantities $x_{\alpha,(2)}$, $x_{\rm c,(2)}$ and $x_{\rm B}$ parametrize the rates of depolarization by optical pumping and collisions, and precession relative to radiative depolarization. They are given by

$$
\begin{aligned}
x_{\alpha,(2)} &= \frac{3.607\pi\lambda_{\rm Ly\alpha}^2\gamma_{\rm 2p}T_*}{AT_\gamma}\tilde{S}_{\alpha,(2)}J_\alpha \\
&= 0.073\tilde{S}_{\alpha,(2)}\left(\frac{1+z}{10}\right)^{-1} \\
&\quad\times\left(\frac{J_\alpha}{10^{-12}{\rm cm}^{-2}{\rm sr}^{-1}{\rm s}^{-1}{\rm Hz}^{-1}}\right),
\end{aligned} \quad (98)
$$

$$
\begin{aligned}
x_{\rm c,(2)} &= \kappa^{(2)}(1\text{-}0)\frac{n_{\rm H}T_*}{AT_\gamma} \\
&= 2\times10^{-3}\left(\frac{1+z}{10}\right)^2\left(\frac{\kappa^{(2)}(1\text{-}0)}{1.3\times10^{-11}{\rm cm}^3{\rm s}^{-1}}\right),\ \text{and}
\end{aligned} \quad (99)
$$

$$
\begin{aligned}
x_{\rm B} &= \frac{g_{\rm e}\mu_{\rm B}T_*}{2\hbar AT_\gamma}B \\
&= 0.698\left(\frac{1+z}{10}\right)^{-1}\left(\frac{B}{10^{-19}{\rm G}}\right).
\end{aligned} \quad (100)
$$

In the equation above, B is the local value of the magnetic field.

We compute the brightness temperature fluctuation, $\delta T_{\rm b}$, from Eq. (90), wherein the phase-space density is given by the sum of the monopole and quadrupole from Eqs. (95) and (97) respectively. We get the following expression, which is one of the main results of this paper:

$$
\begin{aligned}
\delta T_{\rm b}(\hat{\boldsymbol{n}}) = &\, \left(1 - \frac{T_\gamma}{T_{\rm s}}\right)x_{1\rm s}\left(\frac{1+z}{10}\right)^{1/2} \\
&\times\left[26.4\text{ mK}\left\{1 + \left(1 + (\hat{\boldsymbol{k}}\cdot\hat{\boldsymbol{n}})^2\right)\delta\right\}\right. \\
&- 0.128\text{ mK}\left(\frac{T_\gamma}{T_{\rm s}}\right)x_{1\rm s}\left(\frac{1+z}{10}\right)^{1/2} \\
&\times\left\{1 + 2\left(1 + (\hat{\boldsymbol{k}}\cdot\hat{\boldsymbol{n}})^2\right)\delta\right. \\
&\left.\left.- \frac{\delta}{15}\sum_m\frac{4\pi}{5}\frac{Y_{2m}(\hat{\boldsymbol{k}})\left[Y_{2m}(\hat{\boldsymbol{n}})\right]^*}{1 + x_{\alpha,(2)} + x_{\rm c,(2)} - imx_{\rm B}}\right\}\right].
\end{aligned} \quad (101)
$$

Equation (100) offers a rough guide to estimate the strengths of magnetic fields to which the method outlined in this paper is most sensitive. We must keep in mind that the coefficient $x_{\rm B}$ only measures the strength of the

precession relative to radiative de-polarization, and a full analysis of the discriminating power of this method must estimate the sizes of Lyα and collisional de-polarization, or the coefficients $x_{\alpha,(2)}$ and $x_{c,(2)}$ in Eqs. (98) and (99). The second paper in this series studies this in more detail. For now, we note that field strengths of $\mathcal{O}(10^{-19}\ \mathrm{G})$ at redshifts of $z \sim 10$ are associated with $x_B \sim 1$.

Given this scale of field strengths, we identify two physical regimes – one with weaker fields, and one with much stronger ones. We use the weak-field limit of Eq. (101) to make contact with the intuitive picture laid out in Section III. If we consider a magnetic field that is coherent on larger scales than the 21–cm fluctuations of interest and thus effectively homogenous, and take the limit of $x_B \to 0$ in Eq. (101), we obtain the following coordinate independent response to the weak field:

$$\frac{\mathrm{d}\delta T_b}{\mathrm{d}B}(\hat{\boldsymbol{n}}) = 1.786 \times 10^{17}\ \frac{\mathrm{mK}}{\mathrm{G}}\ [\hat{\boldsymbol{B}} \cdot (\hat{\boldsymbol{k}} \times \hat{\boldsymbol{n}})](\hat{\boldsymbol{n}} \cdot \hat{\boldsymbol{k}})$$
$$\times \left(1 - \frac{T_\gamma}{T_s}\right) x_{1s}^2 \left(\frac{T_\gamma}{T_s}\right) \frac{\delta}{(1 + x_{\alpha,(2)} + x_{c,(2)})^2}. \tag{102}$$

In the geometry of Fig. 2, the direction to the observer is $\hat{\boldsymbol{n}} = -\hat{\boldsymbol{y}}$. If we substitute this in the above equation, we recover the angular structure of the correction to the brightness temperature in Section III, in particular, the form of Eq. (10). The latter only accounted for the radiative decay of the magnetic moment, while Eq. (102) includes the additional effect of collisions and optical pumping through the dimensionless factors of $x_{\alpha,(2)}$ and $x_{c,(2)}$.

We realize the complementary strong field limit by taking the limit $x_B \to \infty$ in Eq. (101). The change in brightness temperature over the case with no external magnetic field is

$$\delta T_b(\hat{\boldsymbol{n}})|_{x_B \to \infty} - \delta T_b(\hat{\boldsymbol{n}})|_{x_B=0}$$
$$= 8.53\ \mu\mathrm{K} \times P_2(\hat{\boldsymbol{k}} \cdot \hat{\boldsymbol{B}}) P_2(\hat{\boldsymbol{n}} \cdot \hat{\boldsymbol{B}})$$
$$\times \left(1 - \frac{T_\gamma}{T_s}\right) x_{1s}^2 \left(\frac{1+z}{10}\right) \left(\frac{T_\gamma}{T_s}\right) \frac{\delta}{1 + x_{\alpha,(2)} + x_{c,(2)}}. \tag{103}$$

From the above expression, we see that the effect saturates at large values of the magnetic field strength. However, we observe that it is still possible to reconstruct the direction of the magnetic field in the plane of the sky using the form of the isotropy breaking in $\hat{\boldsymbol{k}}$ space. The correction is roughly three orders of magnitude fainter than the raw 21-cm brightness even for the optimal range of $\hat{\boldsymbol{k}}$, $\hat{\boldsymbol{B}}$, and J_α. However, it should be noted that it is exactly in phase with the conventional brightness temperature fluctuations – that is, it traces the same underlying density field δ and is changing the coefficient in front of this. Thus its effect on the power spectrum is of order 10^{-3}, not 10^{-6} (as would be the case if the magnetic field correction were a new random field, independent of the density but with an amplitude three orders of magnitude smaller).

IX. SUMMARY AND CONCLUSIONS

In this study, we propose a new method to probe magnetic fields present in the universe prior to and during the early stages of cosmic reionization. The method relies on the spin-polarization of the triplet state of the hyperfine sublevels of neutral hydrogen by an anisotropic radiation field near the energy of the 21-cm transition. These anisotropies naturally arise in the early universe due to density fluctuations in the high redshift gas. In the presence of an external magnetic field, the precession of these spin-polarized atoms changes the angular distribution of the emitted 21-cm radiation at second order in optical depth. If the external magnetic fields are coherent over much larger length-scales than the 21-cm fluctuations, they are effectively homogenous and break the isotropy of the signal along the line of sight – this produces a characteristic signature in the two-point correlation function of the brightness-temperature fluctuations.

Due to the long lifetimes of the excited states of the hyperfine transition, this method is naturally optimal for measuring very weak magnetic fields ($\lesssim 10^{-19}$ G at a reference redshift $z \sim 20$, or $\lesssim 10^{-21}$ G in comoving units). It thus raises the exciting possibility of probing seed fields that may have given rise to the magnetic fields observed in the present-day universe. As the background magnetic field increases, the effect saturates; however, even in the saturated case, it is possible to recover the field's direction, and a lower limit on its strength, as discussed in detail in Paper II.

In order to evaluate this effect, we present a detailed calculation of the coupled evolution of atomic and photon density matrices. We account for all the processes which affect the atomic magnetic moments, such as the Wouthuysen-Field effect, atomic collisions, and radiative decay. The main results are Eq. (101), which includes the corrections to the brightness temperature due to all these effects, and Eqs. (102) and (103), which show the weak- and strong-field limits, respectively. This calculation provides a complete theoretical basis for understanding the microphysics of the hyperfine transition in the presence of external magnetic fields, and for calculating the effect of magnetic precession on 21-cm brightness-temperature signal.

The method we proposed here adds to the already exciting opportunities for the use of the 21-cm line as a probe of the early universe, and is in principle sensitive to extremely weak magnetic fields which are far beyond the reach of any other method (including other techniques based on the 21-cm radiation). Paper II of this series [25] presents a formalism to search for evidence of magnetic fields in data from future 21-cm tomography surveys, both using the method presented here, and an extension that is adopted for fields that vary on the survey-scales. In Paper II, we also forecast sensitivity of future surveys to detecting any particular model for magnetic fields (regardless of their origin), and find that an array of dipole antennas, with a collecting area slightly

larger than a square kilometer, is able reach 1σ sensitivity to detecting magnetic fields near saturation ($\sim 10^{-21}$ comoving G at $z \sim 21$), with about three years of integration time.

Appendix A: Conventions for spherical tensors

In this section, we lay out the conventions for spherical tensors we use in the body of the paper, and our reasons for adopting the same.

Consider a passive rotation around the z-axis by an angle α, which connects two coordinate systems S and S' as follows:

$$(\theta, \phi)|_S = (\theta, \phi - \alpha)|_{S'}, \tag{A1}$$

where both sides refer to the same point on the unit sphere. Within quantum mechanics, the coefficients of a state and expectation values of spherical tensors transform with opposite signs:

$$c_m|_{S'} = e^{im\alpha}c_m|_S \quad \text{with} \quad |\psi\rangle = \sum_m c_m|m\rangle \tag{A2}$$

for states and

$$\langle T_m^{(k)}\rangle|_{S'} = e^{-im\alpha}\langle T_m^{(k)}\rangle|_S \tag{A3}$$

for spherical tensors. The spherical tensors of interest are the irreducible components of the matter density matrix ($\mathscr{P}_{jm}$), and the moments of the phase-space density matrix of the radiation [$(f_{\alpha\beta})_{jm}$]. They are defined in Eqs. (13) and (25); these definitions transform in the manner of Eq. (A3).

Note that the definition of the multipoles of the radiation in Eq. (25) differs from the usual convention adopted in cosmology literature, which omits the complex conjugate on its RHS. The latter considers these moments as state-coefficients rather than expectation values of spherical tensors. Considering that the majority of the calculations in this paper have an atomic physics flavor, our definition is convenient, though unconventional.

Appendix B: Spherical Wave Basis for the Radiation's Phase-space Density Matrix

The standard choice of basis for the EM field's expansion is one consisting of plane waves, whose defining characteristic is that they are eigenfunctions of the linear momentum and helicity of the EM field. This is the basis used in Section IV B. However, it is also possible to use eigenstates of the total angular momentum, parity and energy of the EM field as basis elements. This section expands on this, and details how to transform between these two bases.

Eigenstates of total angular momentum have the usual indices j and m. They are classified as electric and magnetic type states depending on how they behave under a parity transformation – electric type states pick up a factor of $(-1)^j$, while those of the magnetic type pick up $(-1)^{j+1}$. The explicit form of these eigenstates is [59]

$$\boldsymbol{A}_{\omega,jm}^{(\lambda)}(\boldsymbol{r}) = \int \frac{\mathrm{d}^3\boldsymbol{k}_\gamma}{(2\pi)^3} \boldsymbol{A}_{\omega,jm}^{(\lambda)}(\boldsymbol{k}_\gamma)e^{i\boldsymbol{k}_\gamma \cdot \boldsymbol{r}}, \quad \lambda = \mathrm{E, M} \tag{B1}$$

$$\boldsymbol{A}_{\omega,jm}^{(\lambda)}(\boldsymbol{k}_\gamma) = 4\pi^2 \left(\frac{\hbar c^3}{\omega^3}\right)^{1/2} \delta(k_\gamma - \omega/c)\boldsymbol{Y}_{jm}^{(\lambda)}(\hat{\boldsymbol{n}}), \text{and}$$
$$\tag{B2}$$

$$\boldsymbol{Y}_{jm}^{(\lambda)}(\hat{\boldsymbol{n}}) = \begin{cases} \frac{1}{\sqrt{j(j+1)}}\nabla_{\hat{\boldsymbol{n}}}Y_{jm} & \lambda = \mathrm{E} \\ \frac{1}{\sqrt{j(j+1)}}\hat{\boldsymbol{n}} \times \nabla_{\hat{\boldsymbol{n}}}Y_{jm} & \lambda = \mathrm{M} \end{cases}, \tag{B3}$$

where $\hat{\boldsymbol{n}} = \hat{\boldsymbol{k}}_\gamma$ is the direction of propagation and the index j runs over integers greater than zero, while m runs over integers from $-j$ to j.

We expand the vector potential $\boldsymbol{A}$ in the same manner as in Eq. (19).

$$\boldsymbol{A}(\boldsymbol{r}) = \sum_{j,m} \int \left[\left\{a_{jm}^{(\mathrm{E})}(\omega)\boldsymbol{A}_{\omega,jm}^{(\mathrm{E})}(\boldsymbol{r}) + a_{jm}^{(\mathrm{M})}(\omega)\boldsymbol{A}_{\omega,jm}^{(\mathrm{M})}(\boldsymbol{r})\right\}\right.$$
$$\left. + \text{h.c.}\right] \mathrm{d}\omega, \tag{B4}$$

where the operators $a_{\omega,jm}^{(e/m)}$ and $a_{\omega,jm}^{(e/m)\dagger}$ are annihilation and creation operators for photons of the electric and magnetic type. Operators for photons of the same type have the following commutation relations:

$$[a_{jm}(\omega), a_{j'm'}^{\dagger}(\omega')] = \delta(\omega - \omega')\delta_{j,j'}\delta_{m,m'} \text{ and}$$
$$[a_{jm}(\omega), a_{j'm'}(\omega')] = [a_{jm}^{\dagger}(\omega), a_{j'm'}^{\dagger}(\omega')] = 0, \tag{B5}$$

while those of different types commute with each other.

The phase-space density matrix in this basis can be defined in the same manner as in Eq. (22) for the plane wave basis:

$$\langle a_{jm}^{(\lambda)\dagger}(\omega)\, a_{j'm'}^{(\lambda')}(\omega')\rangle = f_{m',m}^{(\lambda'j')(\lambda j)}(\omega)\, \delta(\omega - \omega') \tag{B6}$$

for $\lambda, \lambda' = \mathrm{E, M}$.

At this stage, it is worthwhile to examine the general considerations leading to the forms of the density matrices in the two bases. Phase coherence between frequencies separated by $\Delta\omega$ leads to oscillatory features

on time-scales of $\Delta t \sim 1/\Delta \omega$. If the time-interval Δt over which the statistical properties of the radiation field are stationary is sufficiently long, the width of the two-point function in frequency space is $\sim 1/\Delta t \to 0$. Thus the δ-function in the definition in the spherical wave basis [Eq. (B6)] is a consequence of time-translation invariance.

The δ-function in the definition in the plane wave basis [Eq. (22)] is a consequence of invariance under spatial translations, the argument paralleling the one for time-translation invariance above. It is relatively simple to express a state given in the plane wave basis in the spherical one, but the inverse transformation involves averaging over the positions of the interacting atoms to recover translational invariance. This is dealt with in greater detail in Section VII B.

In the rest of this section, we describe the transformation from the plane wave basis (the $f_{X,jm}$s) to the spherical wave one (the $f_{m,m'}^{(\lambda j)(\lambda' j')}$s) centered at the position of a hydrogen atom interacting with the radiation. The transformation is

$$
f_{m,m'}^{(\lambda j)(\lambda' j')}(\omega) = \sum_{\alpha,\beta} \int \mathrm{d}^2 \boldsymbol{n} \, f_{\alpha\beta}(\omega, \hat{\boldsymbol{n}})
$$
$$
\times \left[\boldsymbol{e}_{(\alpha)} \cdot \boldsymbol{Y}_{jm}^{(\lambda)*} \right](\hat{\boldsymbol{n}}) \left[\boldsymbol{e}_{(\beta)}^* \cdot \boldsymbol{Y}_{j'm'}^{(\lambda')} \right](\hat{\boldsymbol{n}}).
$$
(B7)

The normalization is such that if the radiation is unpolarized and isotropic (e.g. a thermal state), the elements of the phase-space density matrix are

$$
f_{m,m'}^{(\lambda j)(\lambda' j')}(\omega) = \begin{cases} f_{\mathrm{I},00}(\omega) \, \delta_{j,j'} \delta_{m,m'} & \text{if } \lambda = \lambda' \\ 0 & \text{if } \lambda \neq \lambda' \end{cases}. \quad \text{(B8)}
$$

We further simplify the angular integral in the transformation of Eq. (B7) using the moments of the phase-space density matrix in the plane wave basis [Eq. (25)], and the Clebsch-Gordan rule for evaluating the angular integral of the product of three spherical harmonics [65].

The M1–M1 block of the phase-space density matrix contributes to the evolution of the atom density matrix [see Section V]. We derive its explicit form for arbitrarily polarized radiation by simplifying Eq. (B7):

$$
f_{m,m'}^{(\mathrm{M1})(\mathrm{M1})}(\omega) = \frac{3}{2} \sum_{j,m_2} \sum_{\alpha,\beta} \alpha\beta(-1)^{\alpha-m'}(f_{\alpha\beta})_{jm_2}(\omega)
$$
$$
\times \begin{pmatrix} 1 & 1 & j \\ -\alpha & \beta & \alpha-\beta \end{pmatrix} \begin{pmatrix} 1 & 1 & j \\ -m & m' & -m_2 \end{pmatrix}.
$$
(B9)

This 3×3 block is equivalently described in terms of its irreducible components $\mathcal{F}_{jm}(\omega)$ of ranks $j = \{0, 1, 2\}$, in exactly the same manner as the matter density matrix $\rho_{m_1 m_2}$ in Eqs. (13) and (15):

$$
\mathcal{F}_{jm}(\omega) = \sqrt{(2j+1)3} \sum_{m_1, m_2} (-1)^{1-m_2} \begin{pmatrix} 1 & j & 1 \\ -m_2 & \mu & m_1 \end{pmatrix}
$$

$$
\times f_{m_1,m_2}^{(\mathrm{M1})(\mathrm{M1})}(\omega), \quad \text{(B10)}
$$

with the inverse relation

$$
f_{m_1 m_2}^{(\mathrm{M1})(\mathrm{M1})}(\omega) = \sum_{jm} \sqrt{\frac{2j+1}{3}}(-1)^{1-m_2} \begin{pmatrix} 1 & j & 1 \\ -m_2 & m & m_1 \end{pmatrix}
$$
$$
\times \mathcal{F}_{jm}(\omega). \quad \text{(B11)}
$$

Substitution in Eq. (B9) gives the explicit forms of these irreducible components

$$
\mathcal{F}_{00}(\omega) = 3 f_{\mathrm{I},00}(\omega), \quad \text{(B12a)}
$$

$$
\mathcal{F}_{1m}(\omega) = \sqrt{\frac{3}{2}} f_{\mathrm{V},1m}(\omega), \text{ and} \quad \text{(B12b)}
$$

$$
\mathcal{F}_{2m}(\omega) = \frac{3}{5\sqrt{2}} \left[f_{\mathrm{I},2m}(\omega) + \sqrt{6} \, f_{\mathrm{E},2m}(\omega) \right]. \quad \text{(B12c)}
$$

Appendix C: Three-point functions of the atoms and the radiation field

Three-point functions of the atom and the radiation field affect the evolution of the atoms' density matrix ρ and the radiation's phase-space density matrix f. In this section, we derive expressions for their contribution.

The unperturbed Hamiltonians for the hydrogen atoms and radiation are

$$
H_{\mathrm{hf}} = E_0 |00\rangle\langle 00| + E_1 \sum_m |1m\rangle\langle 1m|, \quad \text{(C1)}
$$

$$
H_\gamma = \sum_{j,m,\lambda} \int \mathrm{d}\omega \, \hbar\omega \, a_{jm}^{(\lambda)\dagger}(\omega) a_{jm}^{(\lambda)}(\omega), \quad \text{(C2)}
$$

where E_0 and E_1 are the energies of the singlet and triplet levels. The zero-point energy has been left out of Eq. (C2).

A three-point function is the expectation value of an operator consisting of the product of creation and annihilation operators for the hydrogen atoms and for the radiation. This function's evolution is governed by the operator's commutator with the total Hamiltonian:

$$
\frac{\mathrm{d}}{\mathrm{d}t} \left\langle |1m_1\rangle\langle 00| a_{jm}^{(\lambda)}(\omega) \right\rangle
$$
$$
= i(\omega_{\mathrm{hf}} - \omega) \left\langle |1m_1\rangle\langle 00| a_{jm}^{(\lambda)}(\omega) \right\rangle
$$
$$
+ \frac{i}{\hbar} \left\langle \left[H_{\mathrm{hf},\gamma}, |1m_1\rangle\langle 00| a_{jm}^{(\lambda)}(\omega) \right] \right\rangle. \quad \text{(C3)}
$$

Assuming that the interaction is turned on at $t = 0$, the formal solution to Eq. (C3) is

$$
\left\langle |1m_1\rangle\langle 00| a_{jm}^{(\lambda)}(\omega) \right\rangle = \mathcal{C} e^{i(\omega_{\mathrm{hf}} - \omega)t}
$$
$$
+ \frac{i}{\hbar} \int_0^t \mathrm{d}t' e^{-i(\omega_{\mathrm{hf}} - \omega)(t' - t)} \left\langle \left[H_{\mathrm{hf},\gamma}, |1m_1\rangle\langle 00| a_{jm}^{(\lambda)}(\omega) \right] \right\rangle.
$$
(C4)

If the expectation value in the integrand of the second term varies slowly with time, the exponential dominates the integral and results in a δ-function which picks out the frequency resonant with the level gap. This behaves like a rate term when the three-point function is input to an evolution equation (the Fermi golden rule). The first term does not lead to such a secular rate contribution. We have the identity

$$
\left\langle |1m_1\rangle\langle 00|a_{jm}^{(\lambda)}(\omega)\right\rangle
$$
$$
= \frac{i}{\hbar}\pi\delta(\omega - \omega_{\mathrm{hf}})\left\langle \left[H_{\mathrm{hf},\gamma}, |1m_1\rangle\langle 00|a_{jm}^{(\lambda)}(\omega)\right]\right\rangle. \quad \text{(C5)}
$$

We use the form of the interaction Hamiltonian from Eq. (29) to evaluate the last expectation value. Expanding the commutator leads to 4-point functions, which we separate into atom and photon density matrices under the assumption of weak interactions:

$$
\left\langle \left[H_{\mathrm{hf},\gamma}, |1m_1\rangle\langle 00|a_{jm}^{(\lambda)}(\omega)\right]\right\rangle
$$
$$
= \sum_{m_2,m'} V_{m_2 a,m'}^{*}(\omega)\Big[\delta_{m_1 m_2}\,\rho_{aa}\,f_{m,m'}^{(\lambda j),(\mathrm{M1})}(\omega)
$$
$$
- \rho_{m_2 m_1}\Big\{\delta_{(\lambda)(\mathrm{M})}\delta_{j1}\delta_{mm'} + f_{m,m'}^{(\lambda j)(\mathrm{M1})}(\omega)\Big\}\Big]. \quad \text{(C6)}
$$

[1] R. Wielebinski, in *Cosmic Magnetic Fields*, Lecture Notes in Physics, Berlin Springer Verlag, Vol. 664, edited by R. Wielebinski and R. Beck (2005) p. 89.

[2] R. Beck, Space Science Reviews **166**, 215 (2012).

[3] M. L. Bernet, F. Miniati, S. J. Lilly, P. P. Kronberg, and M. Dessauges-Zavadsky, Nature (London) **454**, 302 (2008), arXiv:0807.3347.

[4] J. P. Vallee, New Astronomy Reviews **48**, 763 (2004).

[5] R. Durrer and A. Neronov, Astron. and Astrophys. Review **21**, 62 (2013), arXiv:1303.7121 [astro-ph.CO].

[6] L. M. Widrow, D. Ryu, D. R. G. Schleicher, K. Subramanian, C. G. Tsagas, and R. A. Treumann, Space Science Reviews **166**, 37 (2012), arXiv:1109.4052 [astro-ph.CO].

[7] S. Naoz and R. Narayan, Physical Review Letters **111**, 051303 (2013), arXiv:1304.5792 [astro-ph.CO].

[8] F. Miniati and A. R. Bell, Astrophys. J. **729**, 73 (2011), arXiv:1001.2011 [astro-ph.CO].

[9] T. Kobayashi, Journal of Cosmology and Astroparticle Physics **5**, 040 (2014), arXiv:1403.5168.

[10] D. G. Yamazaki, K. Ichiki, T. Kajino, and G. J. Mathews, Advances in Astronomy **2010** (2010), arXiv:1112.4922 [astro-ph.CO].

[11] P. Blasi, S. Burles, and A. V. Olinto, Astrophysical Journal, Letters **514**, L79 (1999), astro-ph/9812487.

[12] D. Paoletti and F. Finelli, Physics Letters B **726**, 45 (2013), arXiv:1208.2625 [astro-ph.CO].

[13] K. E. Kunze and E. Komatsu, Journal of Cosmology and Astroparticle Physics **1**, 009 (2014), arXiv:1309.7994 [astro-ph.CO].

[14] T. Kahniashvili, Y. Maravin, A. Natarajan, N. Battaglia, and A. G. Tevzadze, Astrophys. J. **770**, 47 (2013), arXiv:1211.2769 [astro-ph.CO].

[15] A. Neronov and I. Vovk, Science **328**, 73 (2010), arXiv:1006.3504 [astro-ph.HE].

[16] F. Tavecchio, G. Ghisellini, L. Foschini, G. Bonnoli, G. Ghirlanda, and P. Coppi, MNRAS **406**, L70 (2010), arXiv:1004.1329 [astro-ph.CO].

[17] K. Dolag, M. Kachelriess, S. Ostapchenko, and R. Tomàs, Astrophysical Journal, Letters **727**, L4 (2011), arXiv:1009.1782 [astro-ph.HE].

[18] A. E. Broderick, P. Chang, and C. Pfrommer, Astrophysical Journal **752**, 22 (2012), arXiv:1106.5494 [astro-ph.CO].

[19] F. Miniati and A. Elyiv, Astrophys. J. **770**, 54 (2013), arXiv:1208.1761 [astro-ph.CO].

[20] L. Sironi and D. Giannios, Astrophys. J. **787**, 49 (2014), arXiv:1312.4538 [astro-ph.HE].

[21] P. Chang, A. E. Broderick, C. Pfrommer, E. Puchwein, A. Lamberts, and M. Shalaby, ArXiv e-prints (2014), arXiv:1410.3797 [astro-ph.HE].

[22] C. D. Dermer, M. Cavadini, S. Razzaque, J. D. Finke, J. Chiang, and B. Lott, Astrophys. J. Lett. **733**, L21 (2011), arXiv:1011.6660 [astro-ph.HE].

[23] A. M. Taylor, I. Vovk, and A. Neronov, Astron. Astrophys. **529**, A144 (2011), arXiv:1101.0932 [astro-ph.HE].

[24] H. Tashiro, W. Chen, F. Ferrer, and T. Vachaspati, Mon. Not. R. Astron. Soc. **445**, L41 (2014), arXiv:1310.4826.

[25] V. Gluscevic, T. Venumadhav, X. Fang, C. Hirata, A. Oklopcic, and A. Mishra, ArXiv e-prints (2016), arXiv:1604.06327.

[26] J. D. Bowman, M. F. Morales, J. N. Hewitt, and MWA Collaboration, in *American Astronomical Society Meeting Abstracts #218* (2011) p. 132.06.

[27] A. R. Parsons, A. Liu, J. E. Aguirre, Z. S. Ali, R. F. Bradley, C. L. Carilli, D. R. DeBoer, M. R. Dexter, N. E. Gugliucci, D. C. Jacobs, P. Klima, D. H. E. MacMahon, J. R. Manley, D. F. Moore, J. C. Pober, I. I. Stefan, and W. P. Walbrugh, Astrophys. J. **788**, 106 (2014), arXiv:1304.4991.

[28] D. R. DeBoer and HERA, in *American Astronomical Society Meeting Abstracts*, American Astronomical Society Meeting Abstracts, Vol. 225 (2015) p. 328.03.

[29] O. Martinez-Rubi, V. K. Veligatla, A. G. de Bruyn, P. Lampropoulos, A. R. Offringa, V. Jelic, S. Yatawatta, L. V. E. Koopmans, and S. Zaroubi, in *Astronomical Data Analysis Software and Systems XXII*, Astronomical Society of the Pacific Conference Series, Vol. 475, edited by D. N. Friedel (2013) p. 377, arXiv:1302.4462 [astro-ph.IM].

[30] L. J. Greenhill and G. Bernardi, ArXiv e-prints (2012), arXiv:1201.1700 [astro-ph.CO].

[31] C. L. Carilli, ArXiv e-prints (2008), arXiv:0802.1727.

[32] D. A. Varshalovich, Astrophysics **4**, 215 (1968).

[33] D. A. Varshalovich, Soviet Physics Uspekhi **13**, 429 (1971).

[34] H. Yan and A. Lazarian, Astrophys. J. **653**, 1292 (2006), astro-ph/0611281.

[35] H. Yan and A. Lazarian, Astrophys. J. **657**, 618 (2007),

astro-ph/0611282.

[36] H. Yan and A. Lazarian, Astrophys. J. **677**, 1401 (2008), arXiv:0711.0926.

[37] J. R. Pritchard and A. Loeb, Reports on Progress in Physics **75**, 086901 (2012), arXiv:1109.6012 [astro-ph.CO].

[38] H. Tashiro and N. Sugiyama, Mon. Not. R. Astron. Soc. **372**, 1060 (2006), astro-ph/0607169.

[39] D. R. G. Schleicher, R. Banerjee, and R. S. Klessen, Astrophys. J. **692**, 236 (2009), arXiv:0808.1461.

[40] M. Shiraishi, H. Tashiro, and K. Ichiki, Phys. Rev. D **89**, 103522 (2014), arXiv:1403.2608.

[41] A. Loeb and M. Zaldarriaga, Physical Review Letters **92**, 211301 (2004), astro-ph/0312134.

[42] P. Madau, A. Meiksin, and M. J. Rees, Astrophys. J. **475**, 429 (1997), astro-ph/9608010.

[43] D. Babich and A. Loeb, Astrophys. J. **635**, 1 (2005), astro-ph/0505358.

[44] S. De and H. Tashiro, Phys. Rev. D **89**, 123002 (2014), arXiv:1307.3584 [astro-ph.CO].

[45] W. Hanle, Naturwissenschaften **11**, 690 (1923).

[46] C. L. Hyder, Astrophys. J. **141**, 1374 (1965).

[47] S. Sahal-Brechot, V. Bommier, and J. L. Leroy, Astron. Astrophys. **59**, 223 (1977).

[48] V. Bommier and S. Sahal-Brechot, Astron. Astrophys. **69**, 57 (1978).

[49] J. O. Stenflo, Solar Physics **80**, 209 (1982).

[50] J. L. Leroy, in *Measurements of Solar Vector Magnetic Fields*, edited by M. J. Hagyard (1985) pp. 121–140.

[51] E. Landi Degl'Innocenti, in *IAU Colloq. 117: Dynamics of Quiescent Prominences*, Lecture Notes in Physics, Berlin Springer Verlag, Vol. 363, edited by V. Ruzdjak and E. Tandberg-Hanssen (1990) pp. 206–230.

[52] V. Bommier, E. Landi Degl'Innocenti, J.-L. Leroy, and S. Sahal-Brechot, Solar Physics **154**, 231 (1994).

[53] A. Omont, Progress in Quantum Electronics **5**, 69 (1977).

[54] P. Goldreich, D. A. Keeley, and J. Y. Kwan, Astrophys. J. **179**, 111 (1973).

[55] P. Goldreich, D. A. Keeley, and J. Y. Kwan, Astrophys. J. **182**, 55 (1973).

[56] P. Goldreich and N. D. Kylafis, Astrophys. J. Lett. **243**, L75 (1981).

[57] H. Yan and A. Lazarian, J. Quant. Spec. Rad. Trans. **113**, 1409 (2012), arXiv:1203.5571 [astro-ph.GA].

[58] K. Blum, *Density Matrix Theory and Applications* (Springer Berlin Heidelberg, 2012).

[59] V. B. Berestetskii, E. M. Lifshitz, and V. B. Pitaevskii, *Relativistic quantum theory. Pt.1* (Pergamon Press, 1971).

[60] M. Zaldarriaga and U. Seljak, Phys. Rev. D **55**, 1830 (1997), astro-ph/9609170.

[61] M. Kamionkowski, A. Kosowsky, and A. Stebbins, Phys. Rev. D **55**, 7368 (1997), astro-ph/9611125.

[62] W. Hu and M. White, Phys. Rev. D **56**, 596 (1997), astro-ph/9702170.

[63] L. Mandel and E. Wolf, *Optical Coherence and Quantum Optics* (Cambridge University Press, 1995).

[64] C. M. Hirata and K. Sigurdson, MNRAS **375**, 1241 (2007), astro-ph/0605071.

[65] D. A. Varshalovich, A. N. Moskalev, and V. K. Khersonskii, *Quantum Theory of Angular Momentum* (World Scientific, Singapore, 1988).

[66] C. M. Hirata, MNRAS **367**, 259 (2006), astro-ph/0507102.

[67] B. Zygelman, Astrophysical Journal **622**, 1356 (2005).

[68] B. Zygelman, Phys. Rev. A **81**, 032506 (2010).

[69] L. C. Balling, R. J. Hanson, and F. M. Pipkin, Phys. Rev. **133**, A607 (1964).

[70] W. Happer, Reviews of Modern Physics **44**, 169 (1972).

[71] Barrat, J.P. and Cohen-Tannoudji, C., J. Phys. Radium **22**, 329 (1961).

[72] C.-P. Ma and E. Bertschinger, Astrophys. J. **455**, 7 (1995), astro-ph/9506072.